Electronic Supplementary Information

Mesomorphic and Dielectric Properties of Strategically Designed Chiral Bent-Core Liquid Crystals Displaying Wide Temperature Range Dark Conglomerate Phase

Anshika Baghla,[†a] Vidhika Punjani,[†a] D.S. Shankar Rao,[*b] S. Krishna Prasad[*b] and Santanu Kumar Pal[*a]

[a]Department of Chemical Sciences, Indian Institute of Science Education and Research (IISER) Mohali, Sector-81, Knowledge City, Manauli-140306, India; E-mail: skpal@iisermohali.ac.in

[b]Centre for Nano and Soft Matter Sciences, Arkavathi, Survey No.7, Shivanapura, Dasanapura Hobli, Bengaluru-562162, India; E-mail: shankar@cens.res.in, skprasad@cens.res.in

Table of contents:

1. Materials and Instrumentation

The chemicals and solvents of analytical reagent (AR) grade were utilized as obtained without undergoing additional purification steps. Separations through column chromatography were conducted using silica gel (with particle sizes of 100-200 mesh and 60-120 mesh). For thin-layer chromatography (TLC), aluminum sheets pre-coated with silica gel (specifically, Merck's Kieselgel 60, F254) were employed.

The details of the instrumentation used for structural characterization (including NMR, HRMS, and FT-IR), thermal analysis (polarized optical microscopy (POM), differential scanning calorimetry (DSC)), and small and wide-angle X-ray scattering (SAXS/WAXS)), dielectric spectroscopy, circular dichroism (CD), atomic force microscopy (AFM) as well as photophysical investigations (UV-vis and fluorescence studies), have been reported earlier[1-3] and are reproduced as below for convenience of the reader:

"Structural characterization of the compounds was carried out through a combination of infrared spectroscopy (IR) (Perkin Elmer Spectrum Two), ^{1}H NMR and ^{13}C NMR (Bruker Biospin Switzerland Avance-iii 400 MHz and 100 MHz spectrometers respectively), UV-vis-NIR spectrophotometers (Agilent Technologies, Cary 5000) and Mass spectrometry (Water Synapt G-2-s QTOF and α-cyano-4-hydroxy-cinnamic acid as a matrix). IR spectra were recorded in neat form for target compounds. ^{1}H NMR spectra were recorded using deuterated chloroform ($CDCl_3$) as solvent and tetramethylsilane (TMS) as an internal standard. The transition temperatures and associated enthalpy values were determined using a differential scanning calorimeter (Perkin Elmer DSC 8000 coupled to a controlled liquid nitrogen accessory (CLN 2)). Textural observations of the mesophase were performed with a Nikon Eclipse LV100POL polarizing optical microscope (POM) provided with a Linkam heating stage (LTS 420). All images were captured using a Q-imaging camera. Small and wide-angle X-ray scattering (SAXS/WAXS) experiments were carried out by filling samples in glass capillaries using Cu-Kα (λ = 1.5418 Å) radiation from Xeuss (Model C HP100 fm) X-ray diffractometer from Xenocs equipped with GeniX 3D source operating at 50 kV and 0.6 mA in conjunction with a multilayer mirror and Pilatus 200 hybrid pixel detector from Dectris. Dielectric spectroscopy measurements were performed using an HP4194A impedance analyzer. Circular Dichroism measurements were performed using JASC0-J810 Spectropolarimeter. The AFM images were captured in tapping mode using an Innova Bruker AFM instrument with an antimony-coated silicon tip measuring 8 nm in radius and image processing was carried out utilizing WSxM software."

2. Synthesis

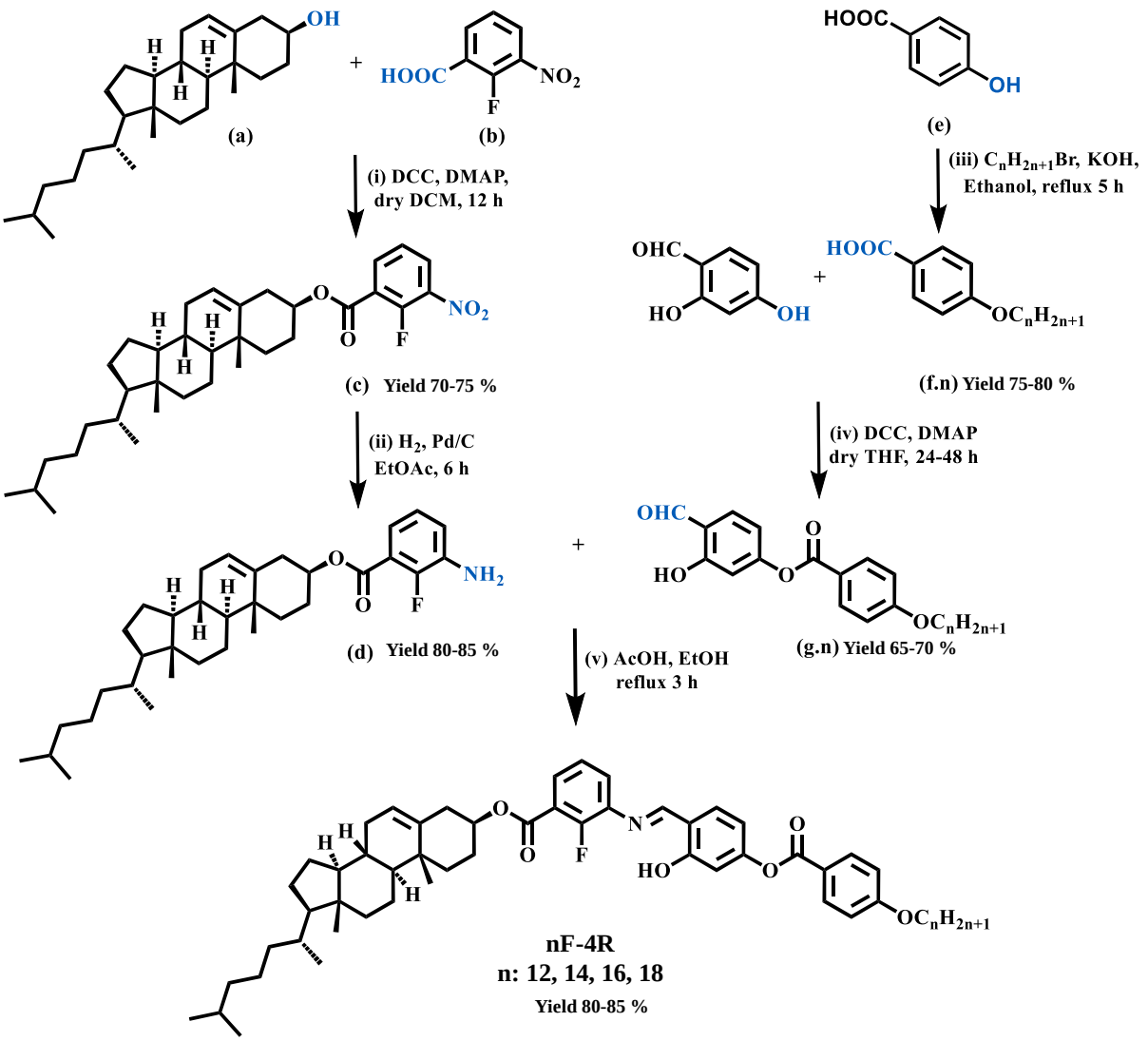

Scheme S1 Synthetic scheme for **nF-4R** series of compounds.

Synthesis of (3S,8S,9S,10R,13R,14S,17R)-10,13-dimethyl-17-((R)-6-methylheptan-2-yl)-2,3,4,7,8,9,10,11,12,13,14,15,16,17-tetradecahydro-1H-cyclopenta[a]phenanthren-3-yl 2-fluoro-3-nitrobenzoate (c)

The compound **(c)** was obtained using Steglich esterification reaction between cholesterol **(a)** and 2-fluoro-3-nitrobenzoic acid **(b)** as follows[2]:

1 equivalent (8.1 mmol) of compound **b** was dissolved in dry dichloromethane (DCM) under nitrogen atmosphere and a catalytic amount of 4-dimethylaminopyridine (DMAP) was added. Further, the addition of 1.25 equivalent (10.1 mmol) of N, N'-dicyclohexylcarbodiimide (DCC) was done and the reaction mixture was allowed to stir for some time. Cholesterol (**a,** 1.1 equivalent, 8.9 mmol) was then added and the reaction mixture was stirred for 12 h. The precipitate of the by-product (Dicyclohexylurea) formed was filtered off and the residue was concentrated using rotatory evaporator. The crude mixture was purified by column

chromatography using silica gel (100-200 mesh) and ethyl acetate-hexane as eluent. The white solid product (**c**) was obtained with 70-75 % yield.

^{1}H NMR (400 MHz, $CDCl_3$, δ in ppm) δ = 8.22 - 8.16 (m, 2H, Ar-H), 7.39 - 7.34 (td, 1H, Ar-H), 5.44 - 5.42 (m, 1H, -CH=C- in cholesteryl), 4.93 - 4.88 (m, 1H, -CH-O- in cholesteryl), 2.50 - 2.47 (m, 2H), 2.05 - 1.98 (m, 3H), 1.98 - 1.91 (m, 1H), 1.87 - 1.74 (m, 2H), 1.62 - 1.57 (m, 2H), 1.56 - 1.49 (m, 3H), 1.48 - 1.37 (m, 3H), 1.36 - 1.26 (m, 3H), 1.25 - 1.02 (m, 11H), 1.01 - 0.93 (m, 2H), 0.91 - 0.86 (m, 8H), 0.69 (s, 3H).

^{13}C NMR (101 MHz, $CDCl_3$, δ in ppm) δ = 162.22, 156.15, 153.06, 139.22, 137.20, 137.18, 129.60, 123.92, 123.22, 122.55, 122.45, 76.31, 56.69, 56.13, 50.02, 42.32, 39.72, 39.53, 38.03, 36.95, 36.63, 36.19, 35.81, 31.93, 31.85, 28.25, 28.03, 27.75, 24.30, 23.84, 22.85, 22.58, 21.06, 19.35, 18.73, 11.87.

Synthesis of (3S,8S,9S,10R,13R,14S,17R)-10,13-dimethyl-17-((R)-6-methylheptan-2-yl)-2,3,4,7,8,9,10,11,12,13,14,15,16,17-tetradecahydro-1H-cyclopenta[a]phenanthren-3-yl 3-amino-2-fluorobenzoate (d)

Compound **c** (1.7 g, 3.2 mmol) was dissolved in ethyl acetate and to it, 5 weight % (85 mg) Palladium on activated charcoal was added as a catalyst. The reaction mixture was then stirred under H_2 gas atmosphere at room temperature. After 6 h, the catalyst was removed by filtration and the residue was concentrated by solvent evaporation to obtain the product **d** (1.4 g) as a brown solid with 80-85 % yield.

^{1}H NMR (400 MHz, $CDCl_3$, δ in ppm) δ = 7.25 - 7.22 (m, 1H, Ar-H), 6.98 - 6.90 (m, 2H, Ar-H), 5.43 - 5.41 (m, 1H, -CH=C- in cholesteryl), 4.89 - 4.82 (m, 1H, -CH-O- in cholesteryl), 3.83 (br s, 2H), 2.48 - 2.45 (m, 2H), 2.04 - 2.00 (m, 2H), 1.98 - 1.94 (m, 1H), 1.94 - 1.81 (m, 2H), 1.74 - 1.68 (m, 1H), 1.54 - 1.45 (m, 4H), 1.35 - 1.33 (m, 3H), 1.28 - 1.23 (m, 2H), 1.21 - 1.09 (m, 7H), 1.06 (br s, 3H), 1.04 - 0.98 (m, 3H), 0.96 - 0.86 (m, 10H), 0.69 (s, 3H).

^{13}C NMR (101 MHz, $CDCl_3$, δ in ppm) δ = 164.13, 139.65, 135.65, 135.52, 123.78, 122.80, 120.44, 119.50, 74.91, 56.70, 56.14, 50.04, 42.33, 39.75, 39.53, 38.15, 37.04, 36.66, 36.20, 35.81, 31.94, 31.88, 28.25, 28.03, 27.83, 24.31, 23.85, 22.84, 22.58, 21.06, 19.38, 18.73, 11.87.

Synthesis of 4-formyl-3-hydroxyphenyl 4-(n-alkoxy)benzoate (g.n)

4-hydroxybenzoic acid (**e**, 1 equivalent) was mixed with an ethanolic solution of 2.5 equivalent KOH under refluxing conditions. To the mixture, 1.2 equivalent of n-alkyl bromide ($C_nH_{2n+1}Br$) was added and allowed to reflux for 5 h. Further, 10 % aqueous KOH was added and the mixture was refluxed for 3 h. The reaction mixture was then neutralized by pouring in acid water and white solid product appeared on stirring. The product was filtrated and washed with water. A yield of 75-80 % was obtained.[4]

4-(n-alkoxy)benzoic acid (**f.n**) was dissolved in dry Tetrahydrofuran (THF) under nitrogen atmosphere and a catalytic amount of DMAP was added. Further, the addition of 1.2 equivalent of DCC was done and the mixture was stirred for some time. 1 equivalent of 2,4-dihydroxybenzaldehyde (**g**) was added after stirring the reaction mixture for 30 minutes. The reaction mixture was then allowed to stir for 48 h at room temperature. The by-product

Dicyclohexylurea (DCU) precipitated out and was removed by filtration. The filtrate was concentrated by evaporating the solvent and the crude product was obtained which was purified by column chromatography using silica gel and hexane-ethyl acetate as eluent. 65-70 % product was yielded. The ^{1}H and ^{13}C NMR data for one of the intermediate homologue (compound **g.12)** is provided below:

^{1}H NMR (400 MHz, $CDCl_3$, δ in ppm) 11.25 (s, 1H, -OH), 9.87 (s, 1H, -CHO), 8.13 - 8.10 (m, 2H, Ar-H), 7.60 (d, *J* = 8.4 Hz, 1H, Ar-H), 6.98 - 6.96 (m, 2H, Ar-H), 6.92 - 6.87 (m, 2H, Ar-H), 4.06 - 4.03 (t, *J* = 6.5 Hz, 2H, -O-CH_2-), 1.85 - 1.78 (m, 2H), 1.51 - 1.43 (m, 2H), 1.37 - 1.27 (m, 16H), 0.90 - 0.86 (t, *J* = 6.7 Hz, 3H, -CH_3 of alkyl chain).

^{13}C NMR (101 MHz, $CDCl_3$, δ in ppm) δ = 195.51, 163.93, 163.91, 163.20, 157.92, 134.94, 132.55, 132.48, 120.70, 118.59, 114.45, 114.19, 110.90, 68.41, 31.93, 29.67, 29.65, 29.61, 29.57, 29.37, 29.08, 25.98, 22.71, 14.15.

Synthesis of (3S,8S,9S,10R,13R,14S,17R)-10,13-dimethyl-17-((R)-6-methylheptan-2-yl)-2,3,4,7,8,9,10,11,12,13,14,15,16,17-tetradecahydro-1H-cyclopenta[a]phenanthren-3-yl 2-fluoro-3-(((E)-4-((4-(hexyloxy)benzoyl)oxy)-2-hydroxybenzylidene)amino)benzoate (nF-4R)

The final step for the synthesis of the **nF-4R** series of compounds involves the formation of a Schiff's base linkage. The compound **g.n** was refluxed in ethanol containing a few drops of glacial acetic acid. An equimolar amount of the amine (**d**) was added to it and the mixture was refluxed for 3 h. The yellow-colored product separated out on cooling. The product was filtered, washed with ethanol, and dried. The obtained yield was 80-85 %. The ^{1}H and ^{13}C NMR data for the final compounds of series **nF-4R** (n : 12, 14, 16, 18) is provided below:

Compound 12F-4R

^{1}H NMR (400 MHz, $CDCl_3$, δ in ppm) δ = 13.22 (s, 1H, -OH), 8.72 (s, 1H, -CH=N-), 8.16 - 8.12 (m, 2H, Ar-H), 7.82 - 7.78 (m, 1H, Ar-H), 7.46 - 7.41 (td, 2H, Ar-H), 7.24 - 7.22 (m, 1H, Ar-H), 6.99 - 6.96 (m, 2H, Ar-H), 6.91 (d, *J* = 2.2 Hz, 1H, Ar-H), 6.87 - 6.84 (dd, 1H, Ar-H), 5.43 (d, *J* = 5.1 Hz, 1H, -CH=C- in cholesteryl), 4.92 - 4.90 (m, 1H, -CH-O- in cholesteryl), 4.07 - 4.03 (t, *J* = 6.6 Hz, 2H, -O-CH_2-), 2.49 (d, *J* = 8.0 Hz, 2H), 2.04 - 1.91 (m, 4H), 1.84 - 1.81 (m, 3H), 1.60 (br s, 1H), 1.52 - 1.44 (m, 7H), 1.35 - 1.33 (m, 6H), 1.27 (br s, 11H), 1.22 - 1.07 (m, 11H), 1.07 - 0.99 (m, 5H), 0.93 - 0.89 (m, 7H), 0.88 - 0.86 (m, 6H), 0.69 (s, 3H).

^{13}C NMR (101 MHz, $CDCl_3$, δ in ppm) δ = 164.30, 163.75, 162.81, 155.47, 139.53, 137.47, 133.57, 132.42, 129.67, 125.22, 124.07, 121.09, 116.91, 114.37, 113.37, 110.86, 75.44, 68.38, 56.70, 56.14, 50.04, 42.33, 39.74, 39.53, 38.13, 37.02, 36.66, 36.20, 35.82, 31.95, 31.88, 29.67, 29.58, 29.38, 29.10, 28.26, 28.04, 27.83, 26.00, 24.31, 23.85, 22.85, 22.72, 22.59, 21.06, 19.38, 18.74, 14.16, 11.88.

HRMS (ESI) m/z: $[M+H]^+$ for $C_{60}H_{82}FNO_6$ calculated = 932.6204, experimental = 932.6194

FT-IR (cm^{-1}): 2920, 2850 (C-H stretching of alkyl groups), 1726 (C=O stretching of ester), 1604 (C=N of imine linkage), 1466, 1251, 1148.

Compound 14F-4R

^{1}H NMR (400 MHz, $CDCl_3$, δ in ppm) δ = 13.22 (s, 1H, -OH), 8.72 (s, 1H, -CH=N-), 8.16 - 8.12 (m, 2H, Ar-H), 7.82 - 7.78 (m, 1H, Ar-H), 7.46 - 7.41 (td, 2H, Ar-H), 7.24 - 7.22 (m, 1H, Ar-H), 6.99 - 6.96 (m, 2H, Ar-H), 6.91 (d, *J* = 2.2 Hz, 2H, Ar-H), 6.87 - 6.84 (dd, 1H, Ar-H), 5.43 (d, *J* = 5.0 Hz, 1H, -CH=C- in cholesteryl), 4.92 - 4.89 (m, 1H, -CH-O- in cholesteryl), 4.07 - 4.03 (t, *J* = 6.6 Hz, 2H, -O-CH_2-), 2.49 (d, *J* = 7.9 Hz, 2H), 2.04 - 1.91 (m, 4H), 1.86 - 1.79 (m, 4H), 1.51 - 1.44 (m, 7H), 1.35 - 1.33 (m, 7H), 1.27 (br s, 15H), 1.22 - 1.09 (m, 8H), 1.07 (br s, 3H), 1.05 - 0.99 (m, 4H), 0.93 - 0.86 (m, 12H), 0.69 (s, 3H).

^{13}C NMR (101 MHz, $CDCl_3$, δ in ppm) δ = 164.55, 164.31, 163.76, 162.81, 155.48, 153.58, 145.66, 139.54, 137.37, 133.57, 132.42, 129.67, 125.23, 124.02, 122.94, 122.92, 121.09, 120.88, 120.79, 116.92, 114.38, 113.38, 110.87, 75.45, 68.39, 56.71, 56.14, 50.04, 42.34, 39.75, 39.53, 38.14, 37.03, 36.67, 36.20, 35.82, 31.95, 31.88, 29.68, 29.62, 29.58, 29.39, 29.11, 28.26, 28.04, 27.83, 26.00, 24.31, 23.85, 22.85, 22.72, 22.59, 21.07, 19.38, 18.74, 14.16, 11.88.

HRMS (ESI) m/z: $[M+H]^+$ for $C_{62}H_{86}FNO_6$ calculated = 960.6518, experimental = 960.6533

FT-IR (cm^{-1}): 2920, 2851 (C-H stretching of alkyl groups), 1726 (C=O stretching of ester), 1604 (C=N of imine linkage), 1467, 1252, 1149.

Compound 16F-4R

^{1}H NMR (400 MHz, $CDCl_3$, δ in ppm) δ = 13.22 (s, 1H, -OH), 8.72 (s, 1H, -CH=N-), 8.16 - 8.13 (m, 2H, Ar-H), 7.82 - 7.78 (m, 1H, Ar-H), 7.46 - 7.41 (m, 2H, Ar-H), 7.24 - 7.22 (m, 1H, Ar-H), 6.99 - 6.97 (m, 2H, Ar-H), 6.91 (d, *J* = 2.2 Hz, 1H, Ar-H), 6.87 - 6.84 (dd, 1H, Ar-H), 5.43 (d, *J* = 4.8 Hz, 1H, -CH=C- in cholesteryl), 4.95 - 4.87 (m, 1H, -CH-O- in cholesteryl), 4.07 - 4.03 (t, *J* = 6.6 Hz, 2H, -O-CH_2-), 2.49 (d, *J* = 8.1 Hz, 2H), 2.04 - 1.91 (m, 4H), 1.86 - 1.75 (m, 4H), 1.60 - 1.54 (m, 1H), 1.51 - 1.44 (m, 6H), 1.44 - 1.35 (m, 3H), 1.26 (br s, 24H), 1.22 - 1.09 (m, 7H), 1.07 (br s, 4H), 1.05 - 0.99 (m, 4H), 0.93 - 0.86 (m, 12H), 0.69 (s, 3H).

^{13}C NMR (101 MHz, $CDCl_3$, δ in ppm) δ = 164.50, 164.29, 163.75, 162.81, 156.09, 155.47, 139.53, 136.19, 133.57, 132.42, 129.67, 125.22, 123.89, 122.61, 121.09, 116.91, 114.37, 113.37, 110.86, 75.43, 68.38, 56.70, 56.14, 50.04, 42.33, 39.74, 39.53, 38.13, 37.03, 36.66, 36.20, 35.82, 31.95, 31.88, 29.72, 29.69, 29.62, 29.59, 29.39, 29.11, 28.26, 28.04, 27.83, 26.00, 24.31, 23.85, 22.86, 22.72, 22.59, 21.07, 19.38, 18.74, 14.16, 11.88.

HRMS (ESI) m/z: $[M+H]^+$ for $C_{64}H_{90}FNO_6$ calculated = 988.6831, experimental = 988.6846

FT-IR (cm^{-1}): 2920, 2850 (C-H stretching of alkyl groups), 1726 (C=O stretching of ester), 1605 (C=N of imine linkage), 1467, 1251, 1149.

Compound 18F-4R

^{1}H NMR (400 MHz, $CDCl_3$, δ in ppm) δ = 13.22 (s, 1H, -OH), 8.72 (s, 1H, -CH=N-), 8.14 (d, *J* = 8.4 Hz, 2H, Ar-H), 7.82 - 7.79 (t, *J* = 6.8 Hz, 1H, Ar-H), 7.46 - 7.42 (t, *J* = 8.3 Hz, 2H, Ar-H), 7.24 - 7.22 (m, 1H, Ar-H), 6.98 (d, *J* = 8.5 Hz, 2H, Ar-H), 6.91 (br s, 1H, Ar-H), 6.86 -

6.84 (m, 1H, Ar-H), 5.44 (br s, 1H, -CH=C- in cholesteryl), 4.92 (m, 1H, -CH-O- in cholesteryl), 4.07 - 4.03 (t, J = 6.6 Hz, 2H, -O-CH_2-), 2.49 (d, J = 8.2 Hz, 2H), 2.04 - 1.91 (m, 5H), 1.84 - 1.75 (m, 5H), 1.54 - 1.46 (m, 6H), 1.35 - 1.33 (m, 6H), 1.26 (br s, 27H), 1.14 - 0.99 (m, 12H), 0.93 - 0.86 (m, 12H), 0.69 (s, 3H).

^{13}C NMR (101 MHz, $CDCl_3$, δ in ppm) δ = 164.47, 164.46, 164.29, 163.75, 163.66, 162.80, 155.78, 155.46, 153.49, 139.52, 137.33, 133.57, 132.42, 129.69, 125.18, 124.07, 122.96, 121.08, 120.85, 120.75, 116.91, 114.37, 113.36, 110.85, 75.43, 68.38, 56.70, 56.14, 50.04, 42.33, 39.74, 39.54, 38.14, 37.02, 36.66, 36.20, 35.83, 31.96, 31.87, 29.74, 29.70, 29.63, 29.60, 29.41, 29.11, 28.27, 28.04, 27.83, 26.01, 24.32, 23.86, 22.86, 22.73, 22.60, 21.07, 19.38, 18.74, 14.17, 11.88.

HRMS (ESI) m/z: $[M+H]^+$ for $C_{66}H_{94}FNO_6$ calculated = 1016.7144, experimental = 1016.7142

FT-IR (cm^{-1}): 2920, 2851 (C-H stretching of alkyl groups), 1727 (C=O stretching of ester), 1606 (C=N of imine linkage), 1466, 1254, 1152.

3. Chemical Characterization

^{1}H and ^{13}C NMR

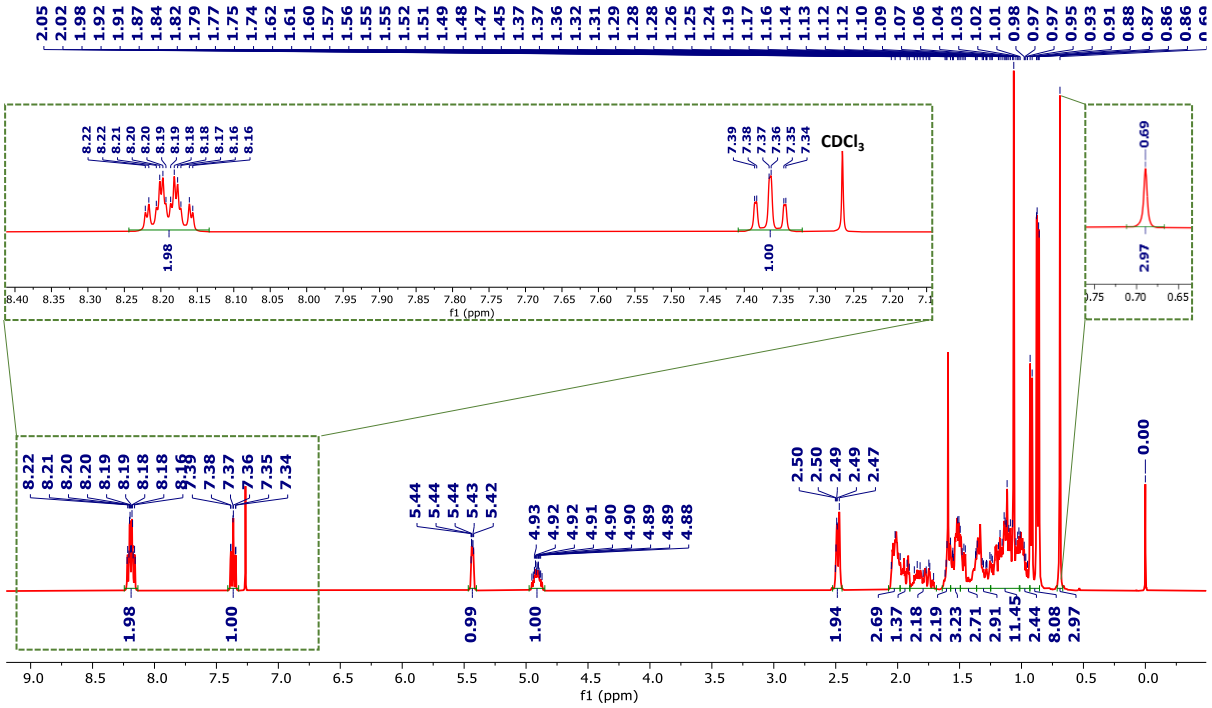

Fig. S1 ^{1}H NMR spectrum for compound **c**.

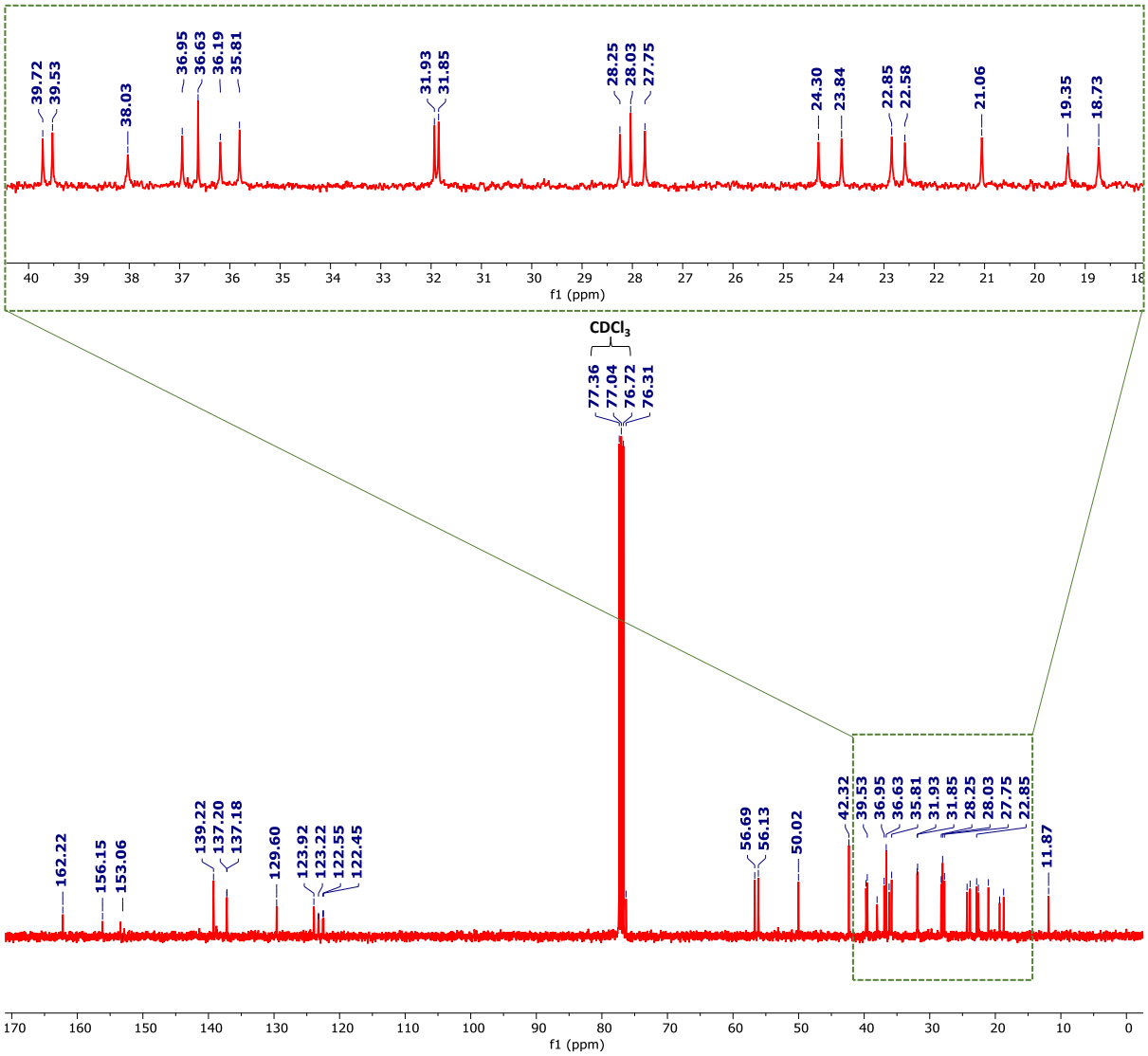

Fig. S2 ^{13}C NMR spectrum for compound **c**.

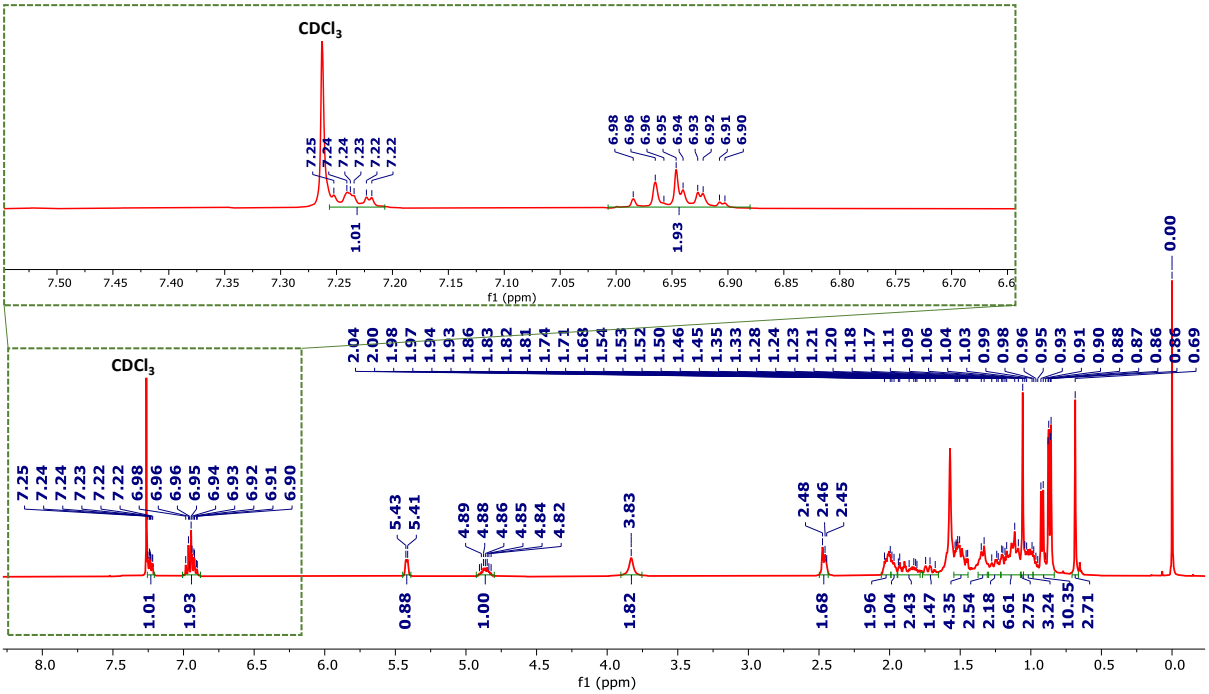

Fig. S3 ^{1}H NMR spectrum for compound **d**.

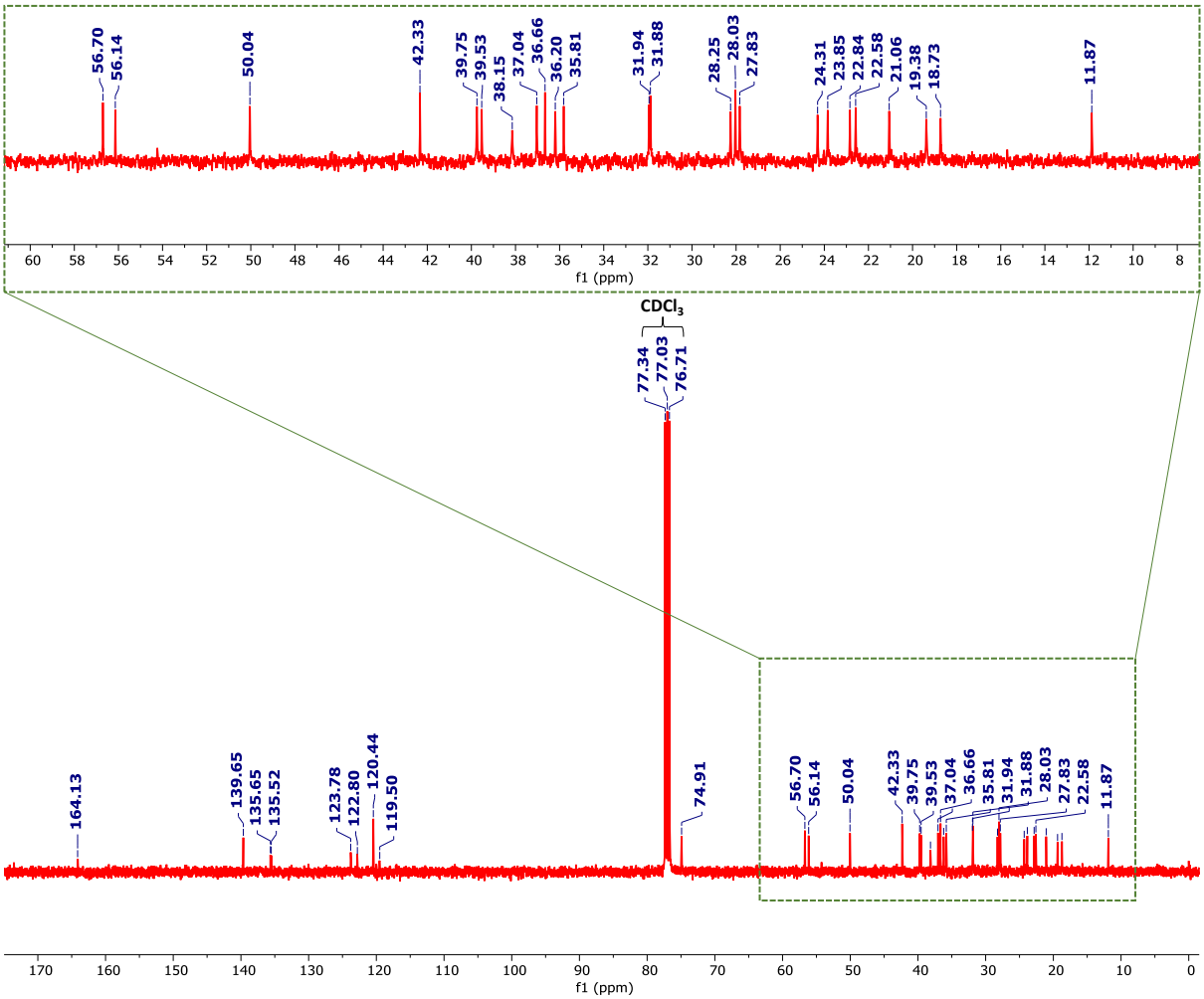

Fig. S4 ^{13}C NMR spectrum for compound **d**.

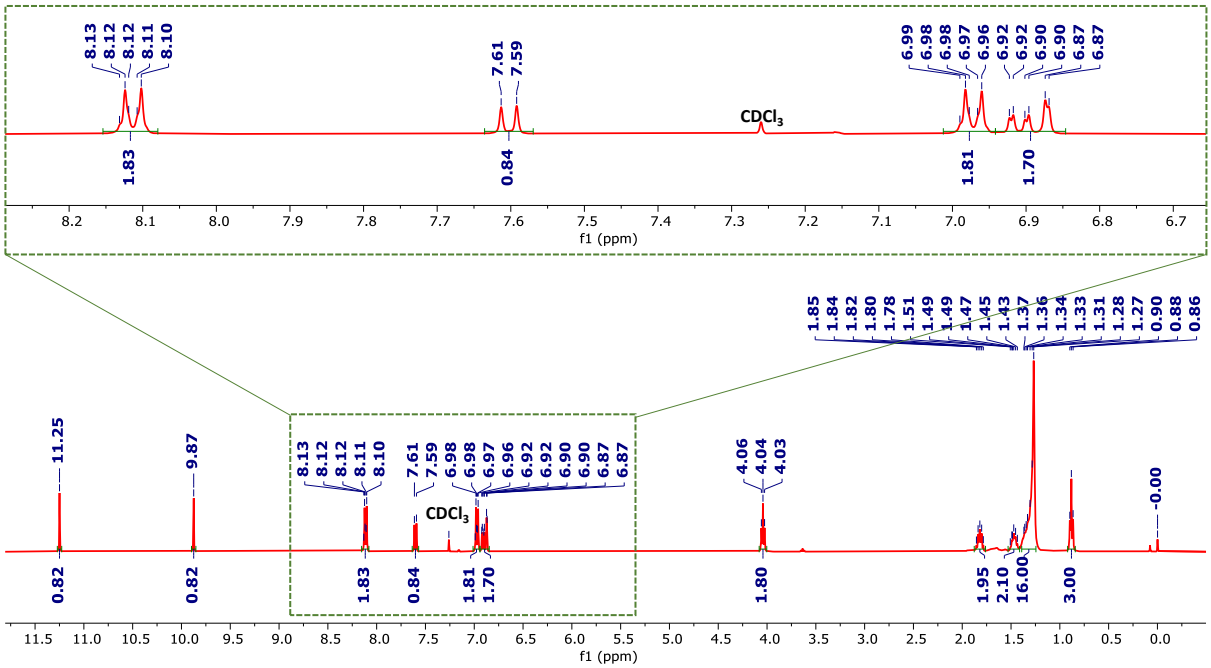

Fig. S5 ^{1}H NMR spectrum for compound **g.12**.

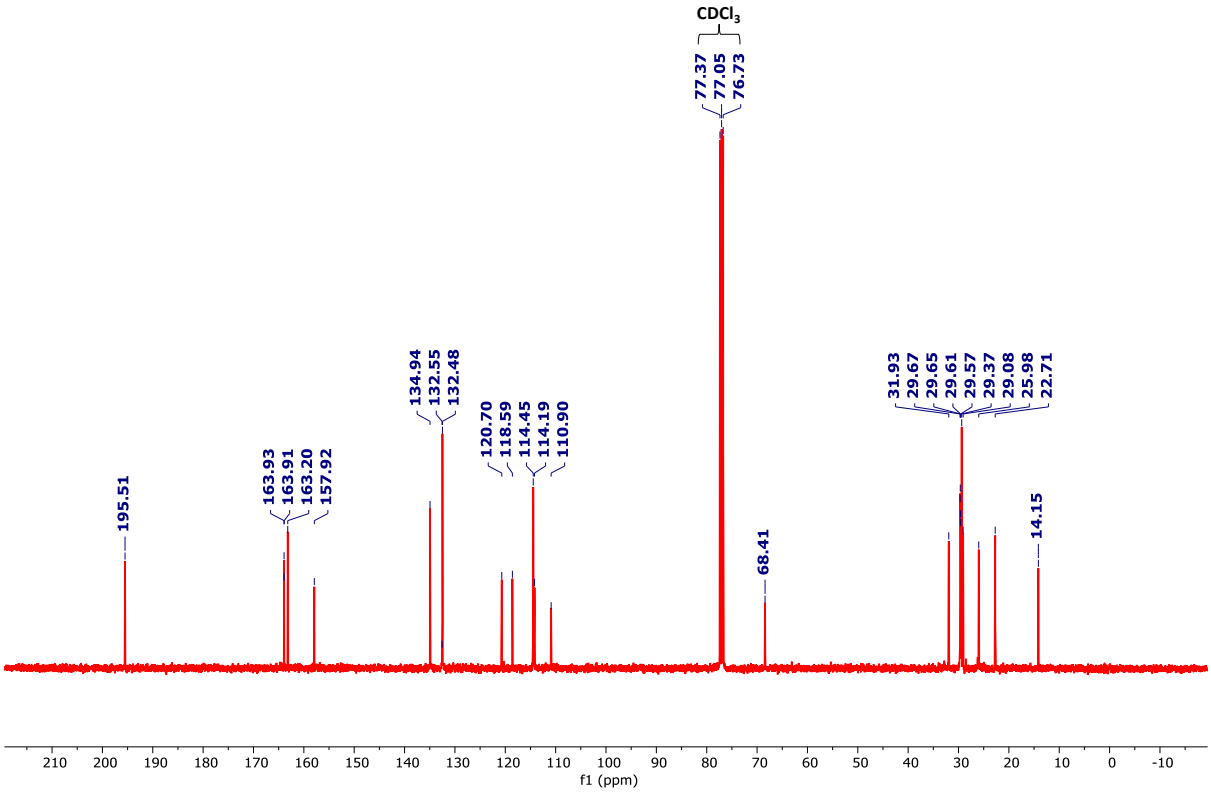

Fig. S6 ^{13}C NMR spectrum for compound **g.12**.

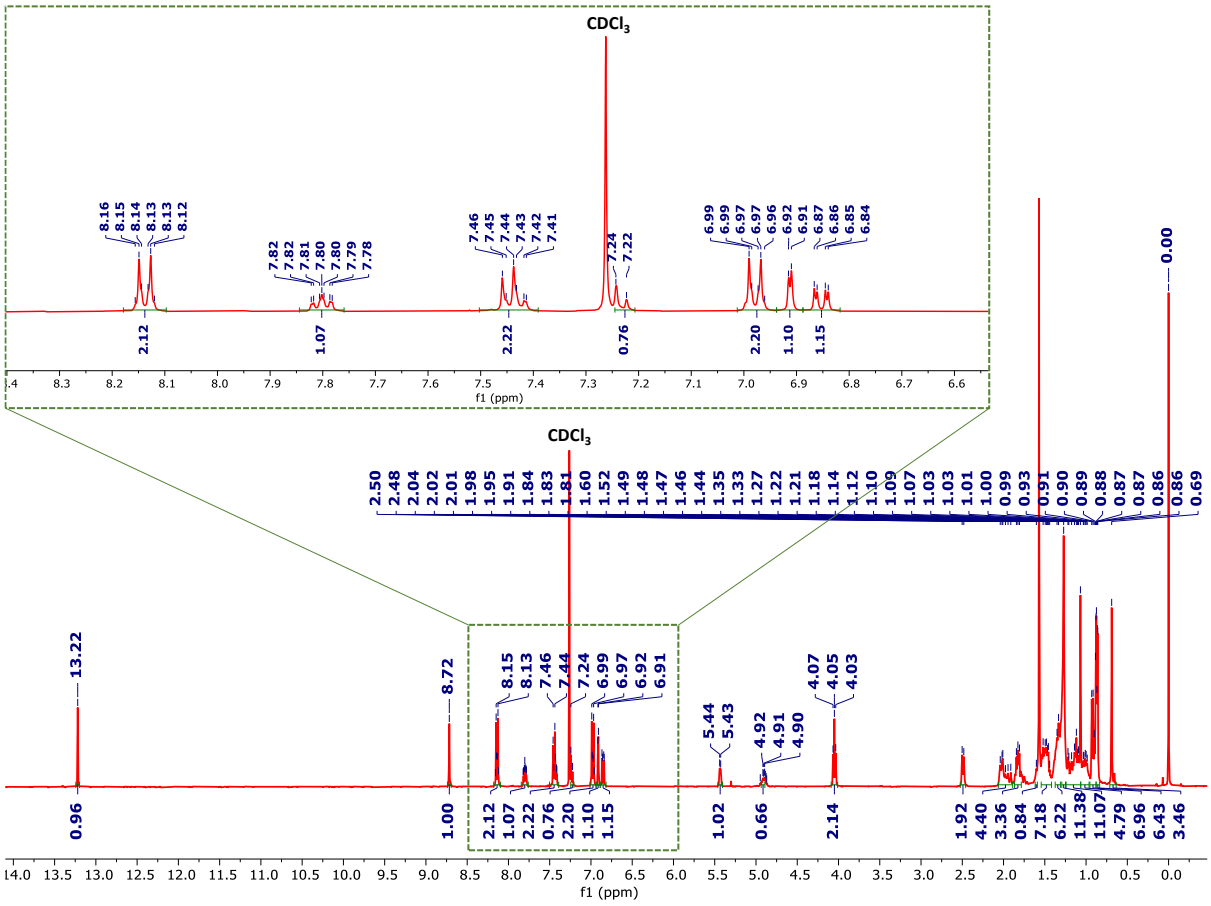

Fig. S7 ^{1}H NMR spectrum for compound **12F-4R.**

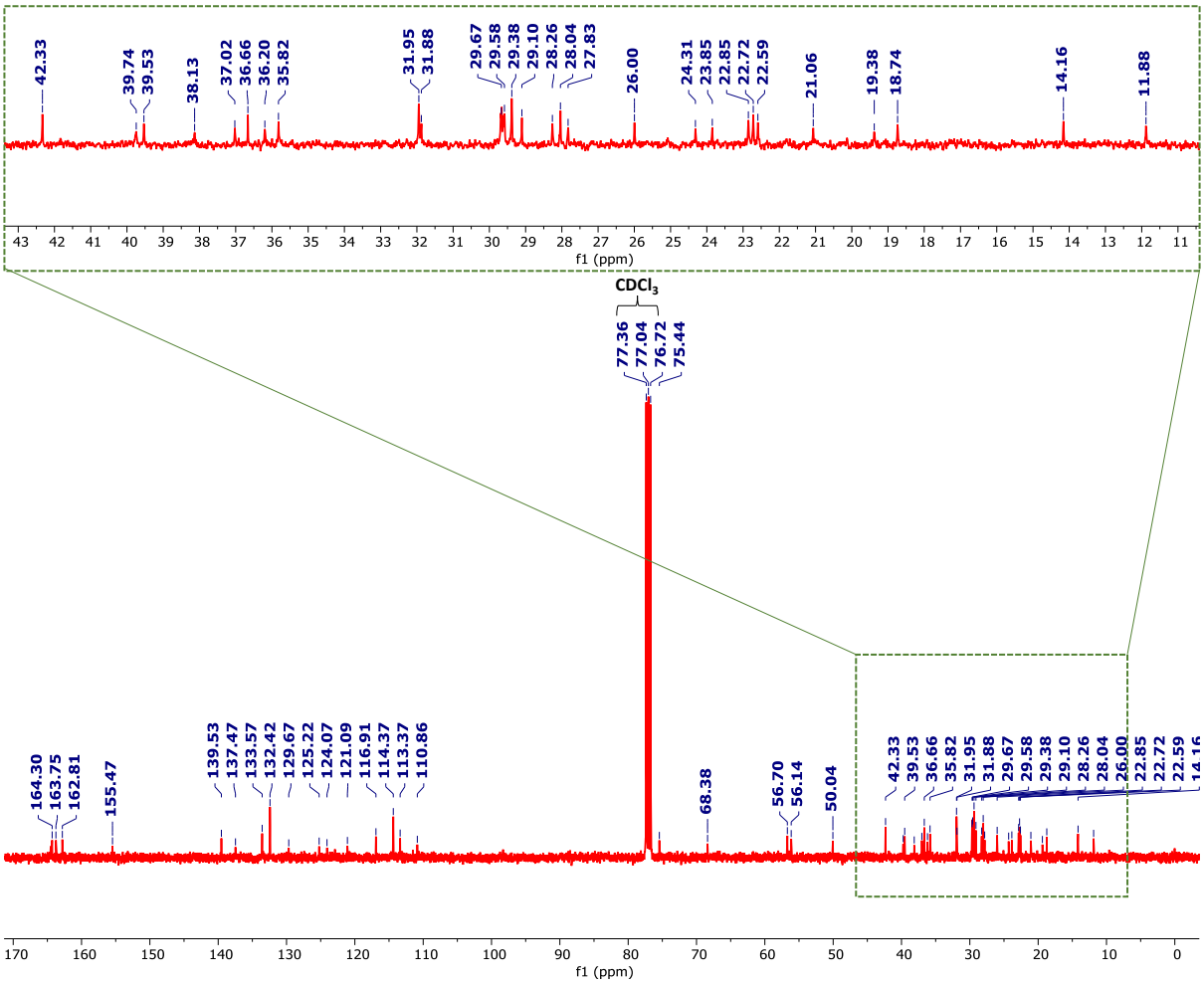

Fig. S8 ^{13}C NMR spectrum for compound **12F-4R.**

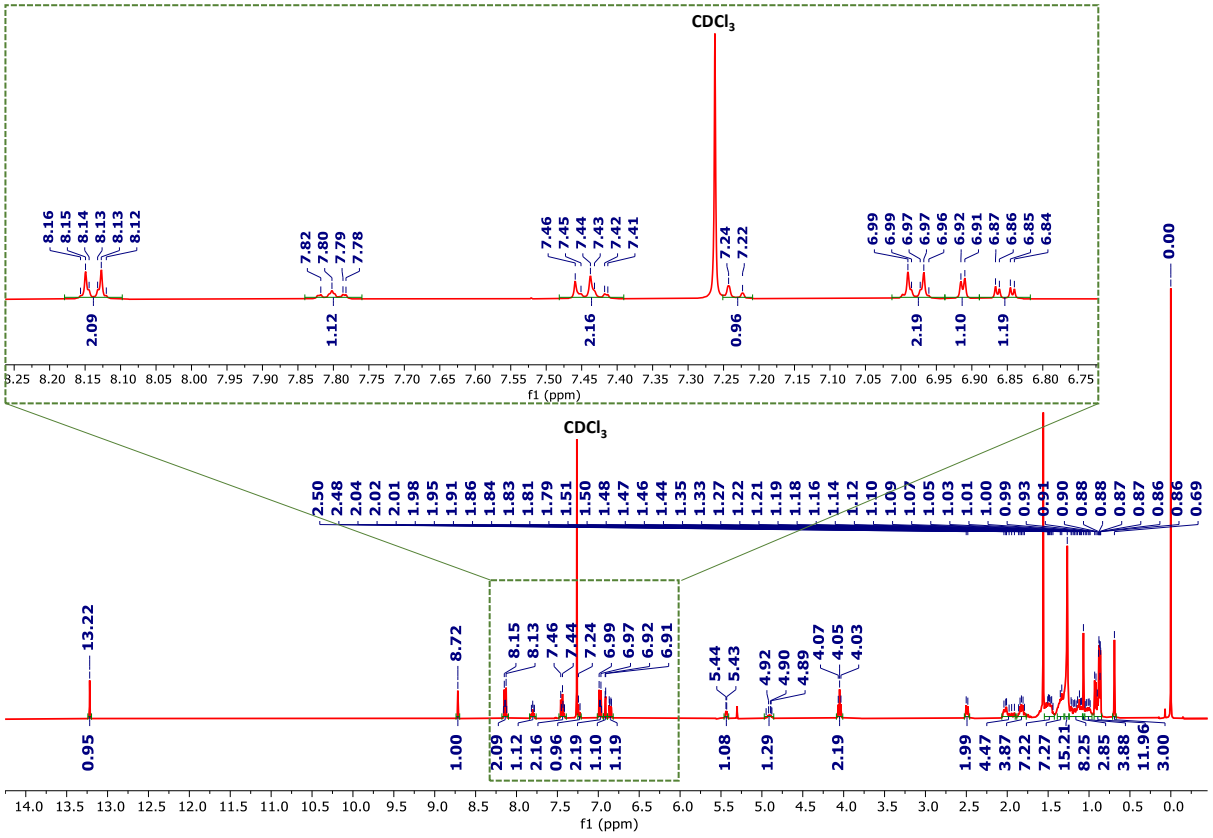

Fig. S9 ^{1}H NMR spectrum for compound **14F-4R.**

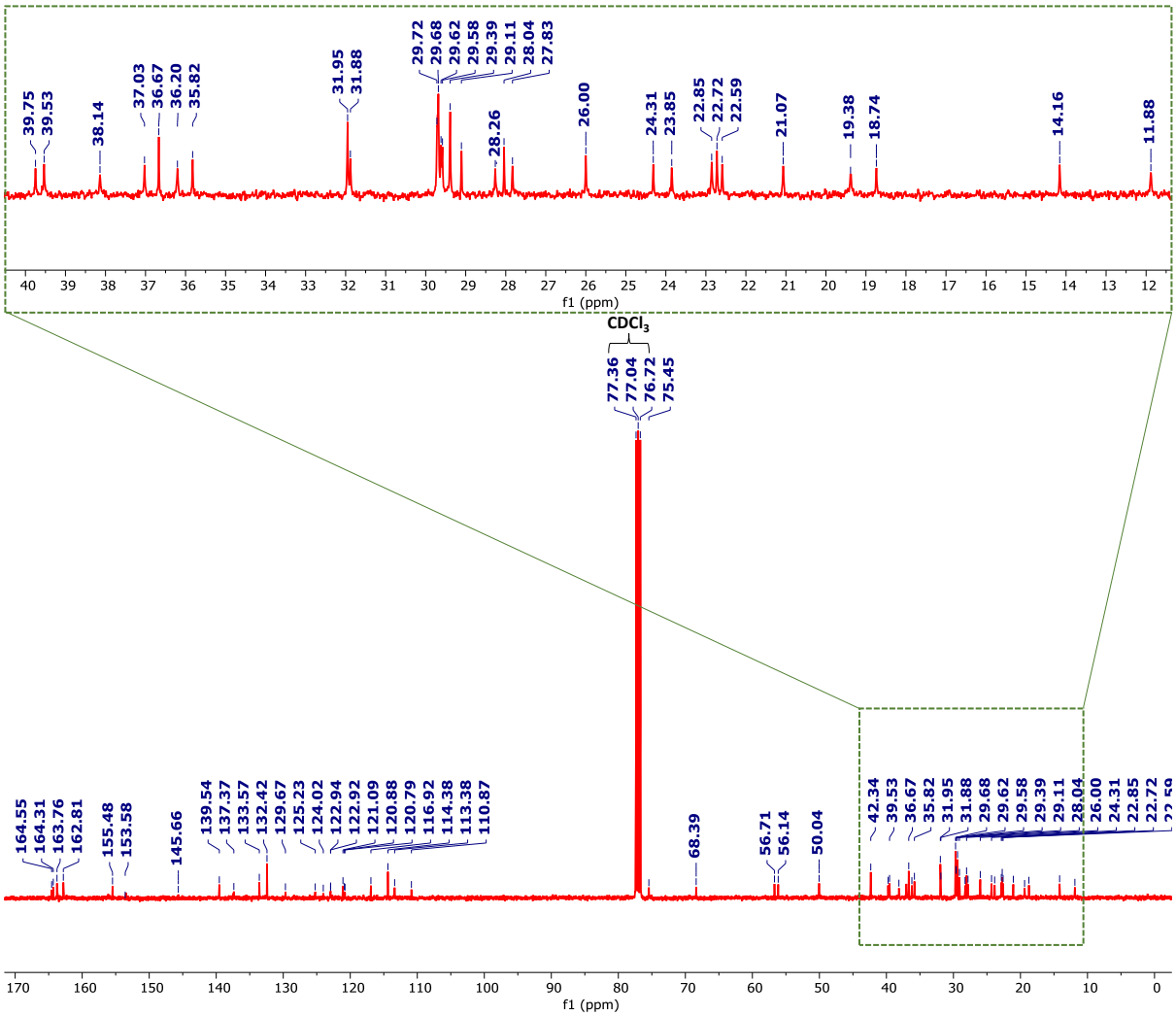

Fig. S10 ^{13}C NMR spectrum for compound **14F-4R.**

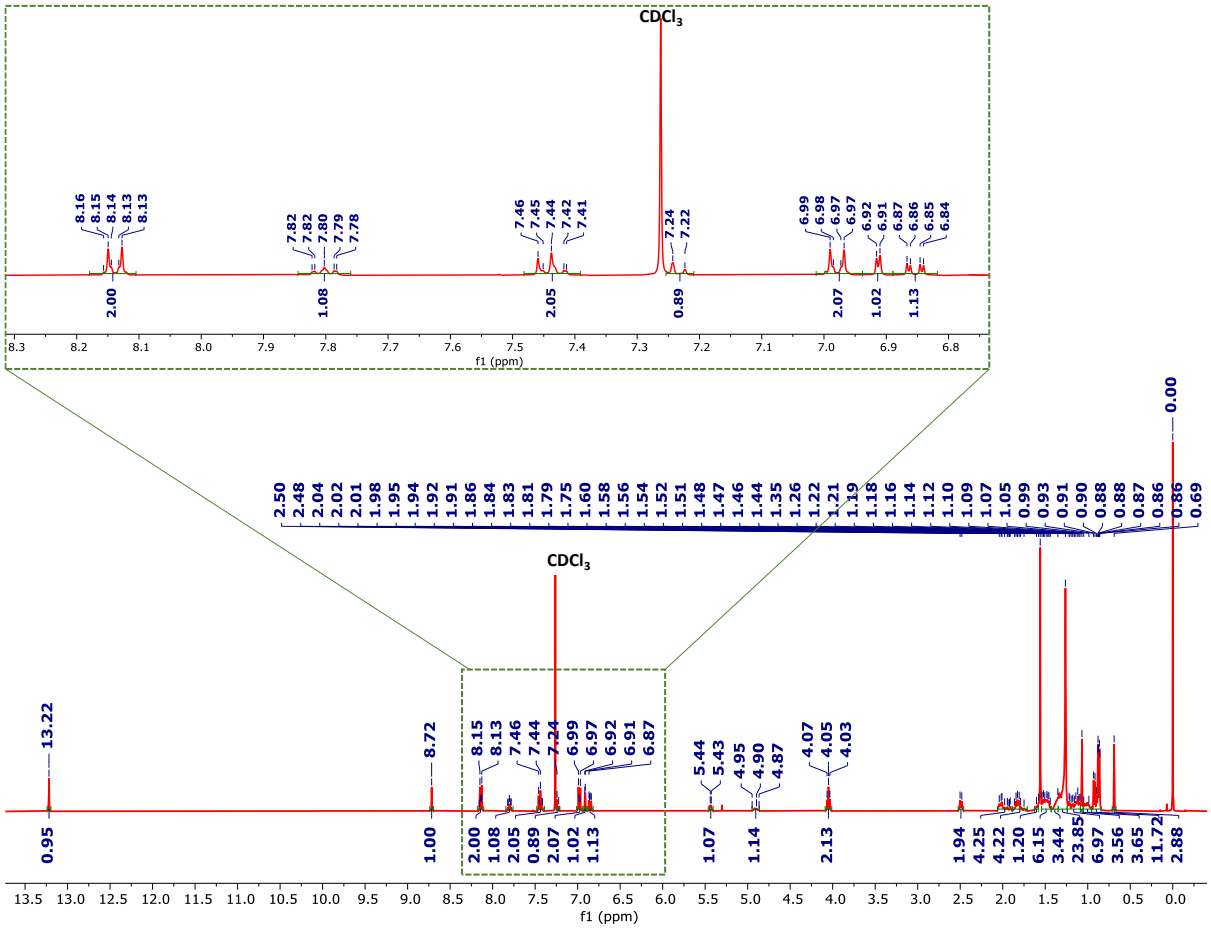

Fig. S11 ^{1}H NMR spectrum for compound **16F-4R.**

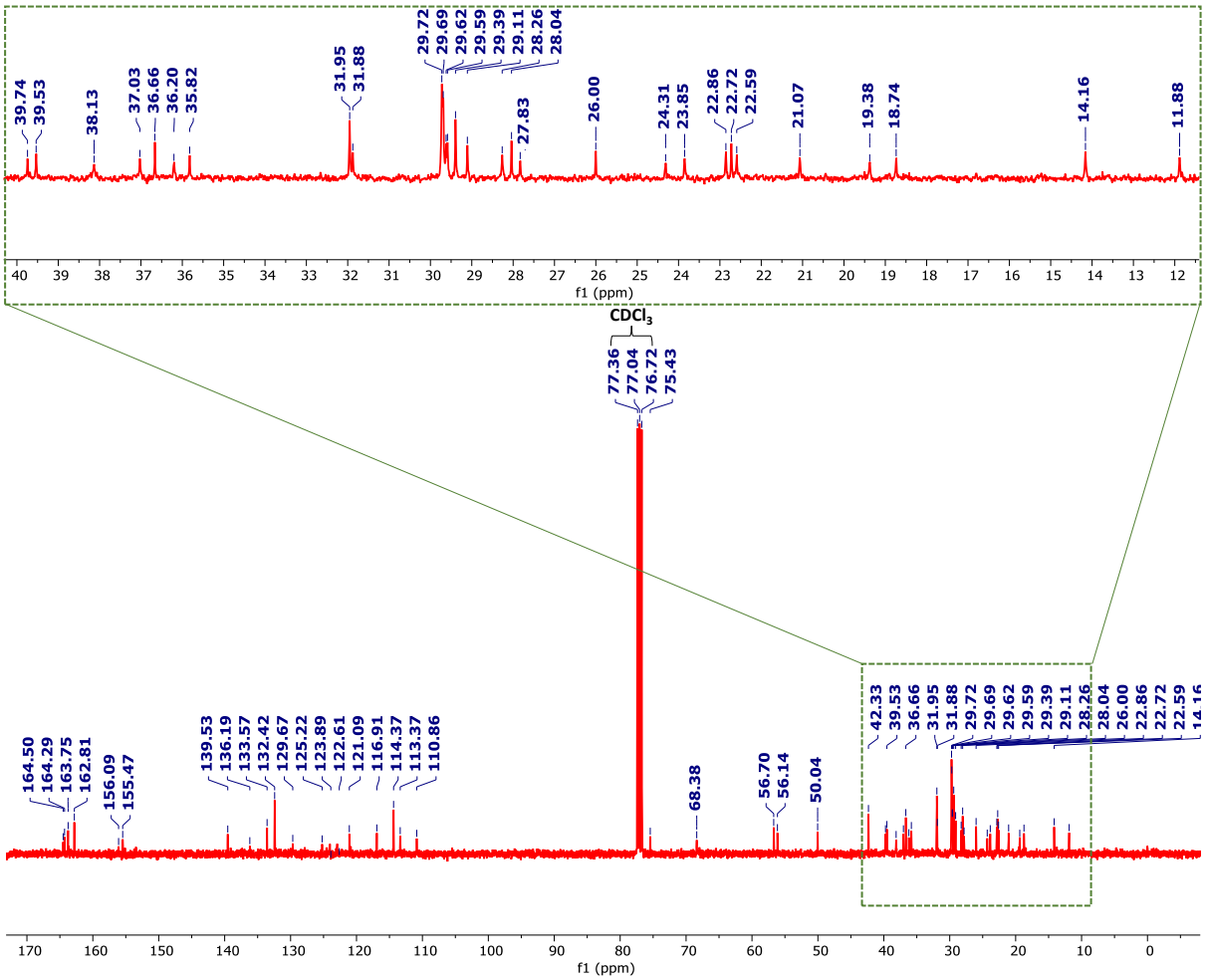

Fig. S12 ^{13}C NMR spectrum for compound **16F-4R.**

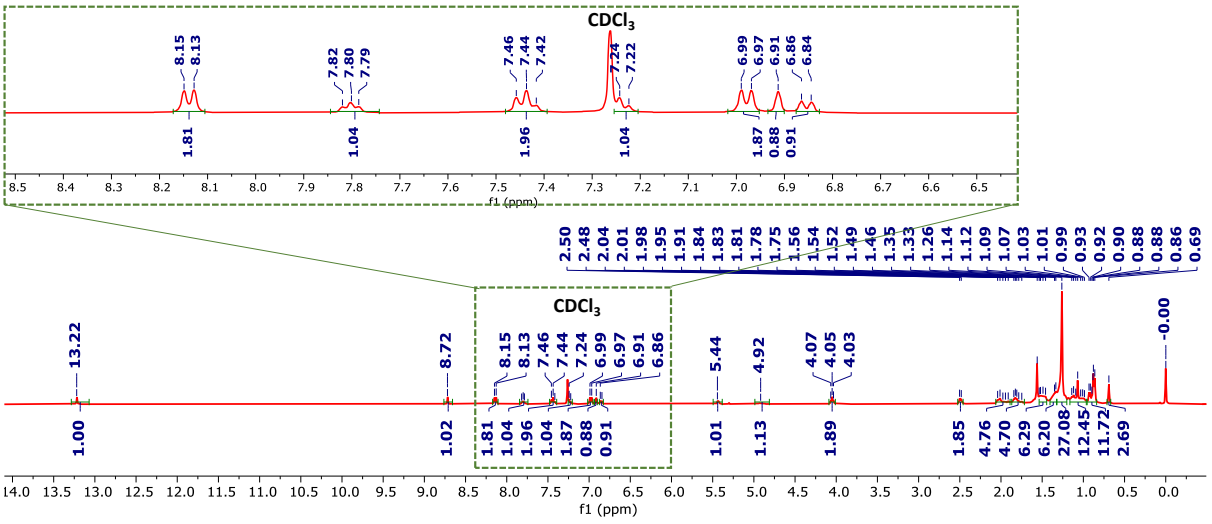

Fig. S13 ^{1}H NMR spectrum for compound **18F-4R.**

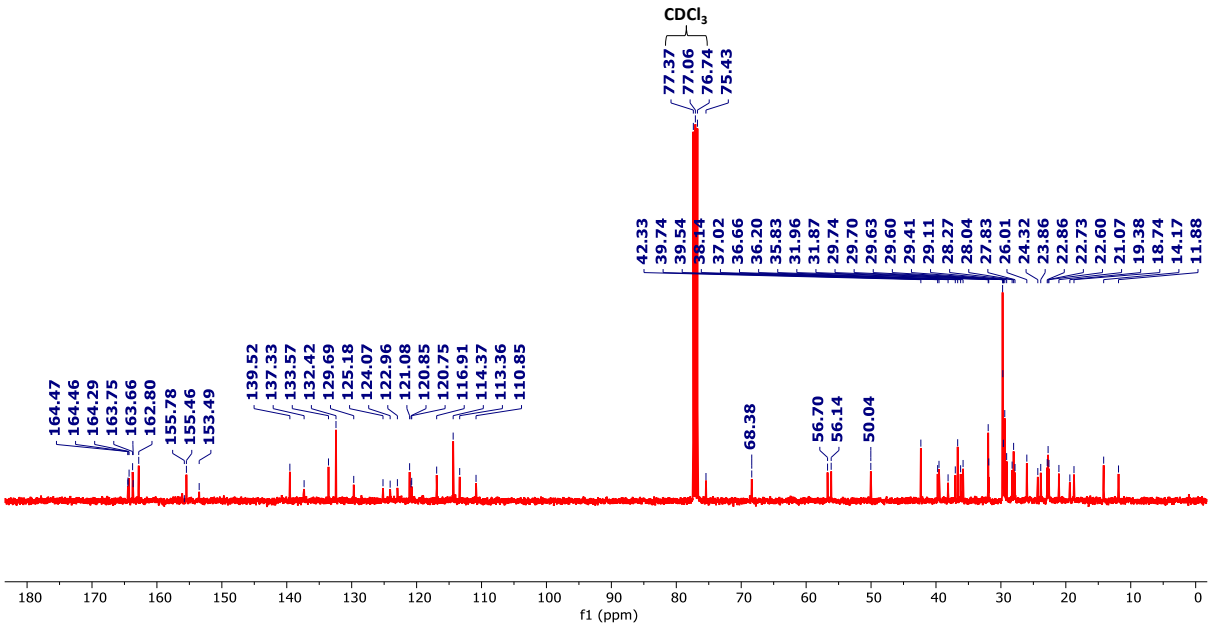

Fig. S14 ^{13}C NMR spectrum for compound **18F-4R.**

HRMS

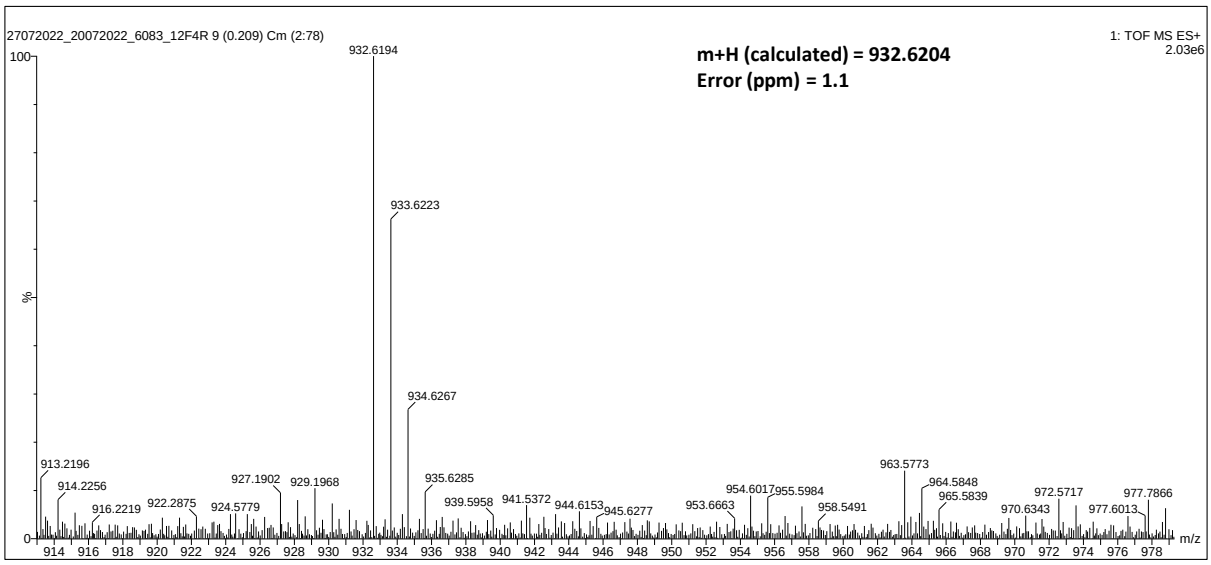

Fig. S15 ESI spectrum for compound **12F-4R.**

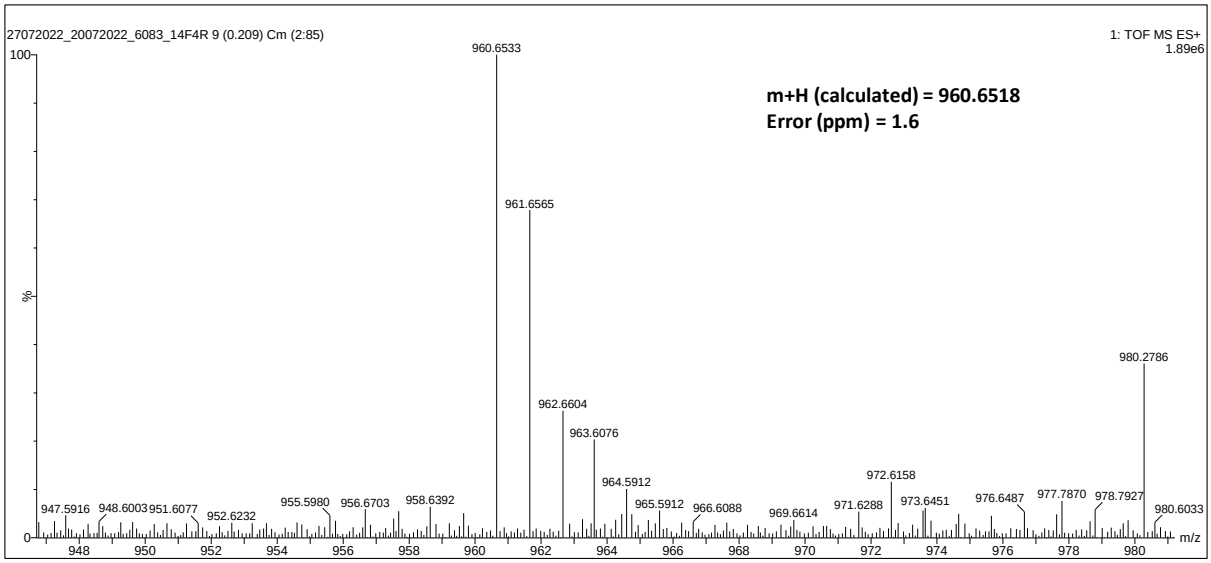

Fig. S16 ESI spectrum for compound **14F-4R.**

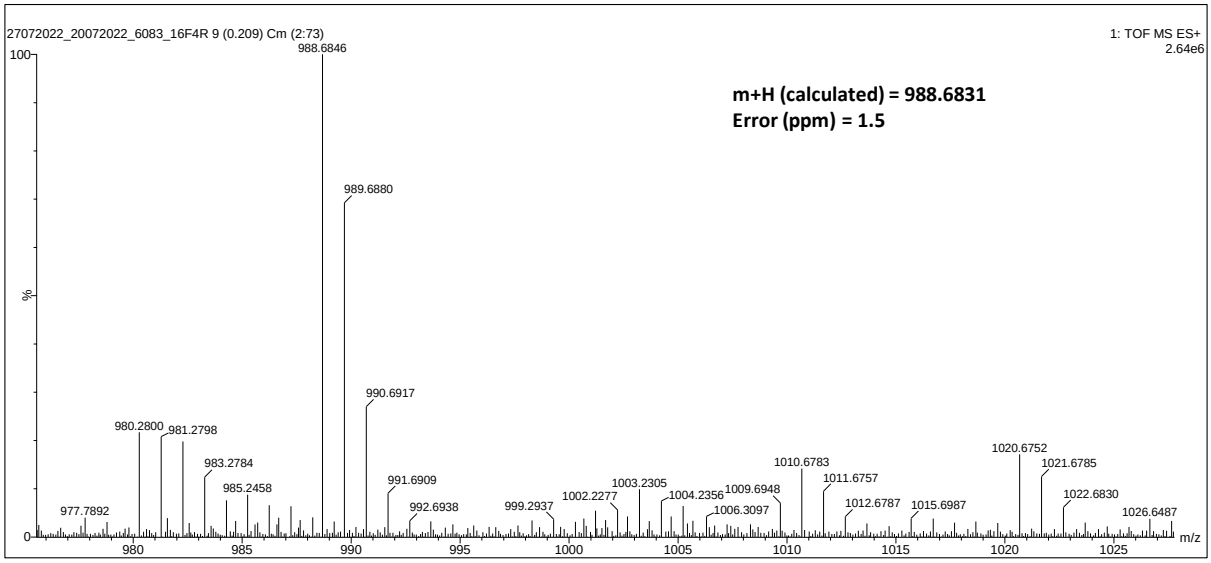

Fig. S17 ESI spectrum for compound **16F-4R.**

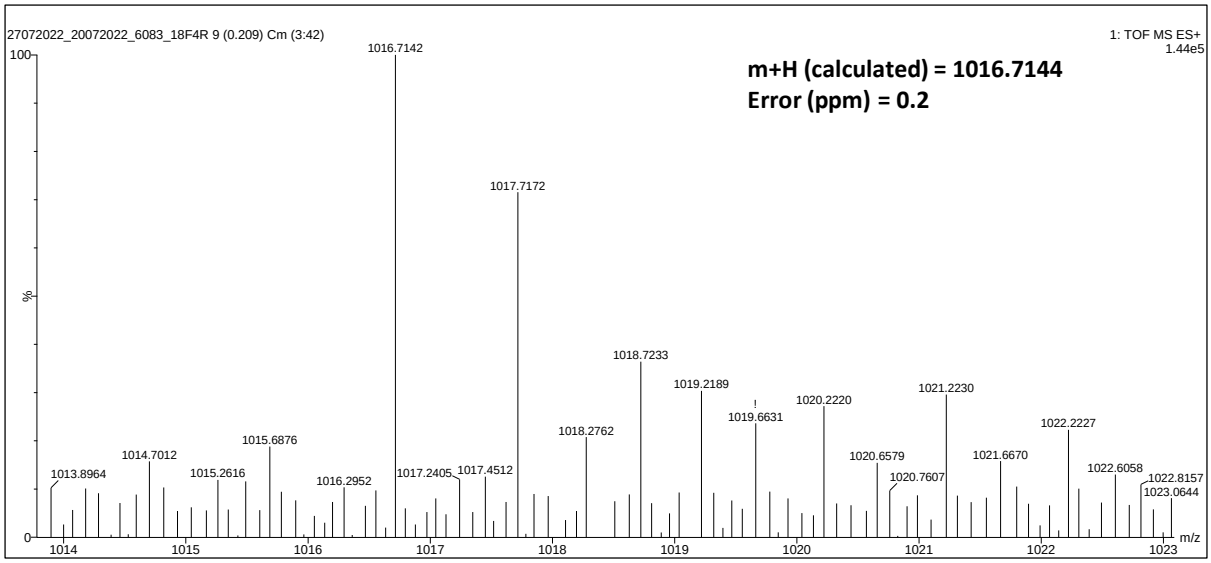

Fig. S18 ESI spectrum for compound **18F-4R.**

4. Polarized Optical Microscopy

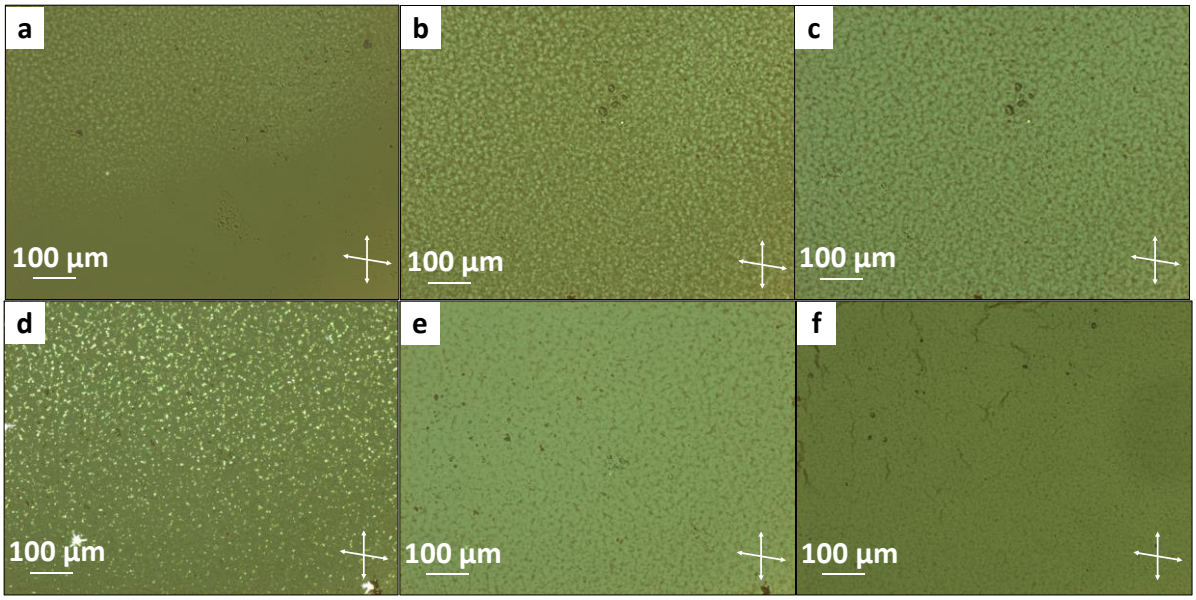

Fig. S19 POM images (under uncrossed polarizers by 4°, 100X magnification, cooling rate 5 °C/min) for the compound **12F-4R** on an untreated glass slide (a) appearance of domains on cooling from isotropic liquid, at 187 °C (b) at 175.3 °C (c) at 145 °C (d) crystal at 96 °C. Upon heating after crystallization, domains reappeared (e) at 145.5 °C (f) at 174.8 °C.

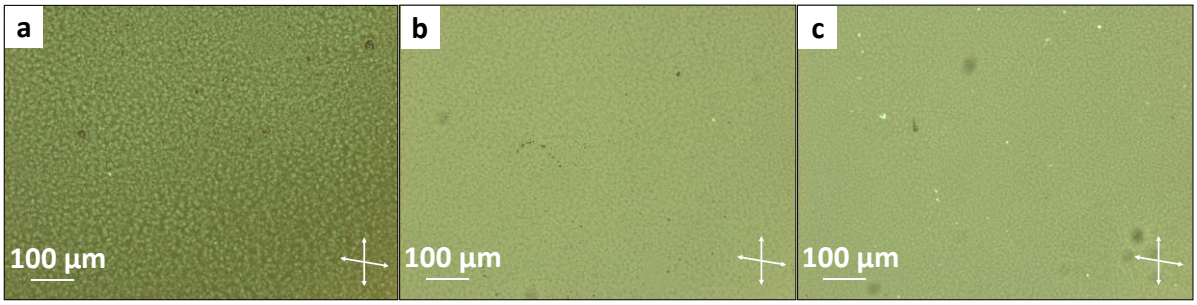

Fig. S20 POM images for the compound (a) **12F-4R** at 180.5 °C (b) **16F-4R** at 168.9 °C (c) **18F-4R** at 183.8 °C on an untreated glass slide (100X magnification, uncrossed polarizers by an angle of 5°).

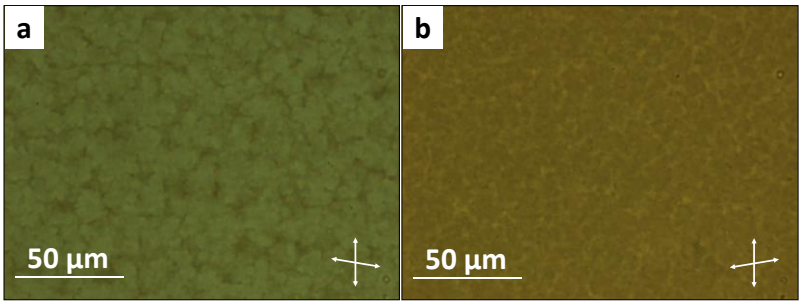

Fig. S21 (a) and (b) POM images showing opposite chirality domains respectively, for compound **12F-4R** on an untreated glass slide (164.8 °C, 500X magnification) between uncrossed polarizers by an angle of 6°.

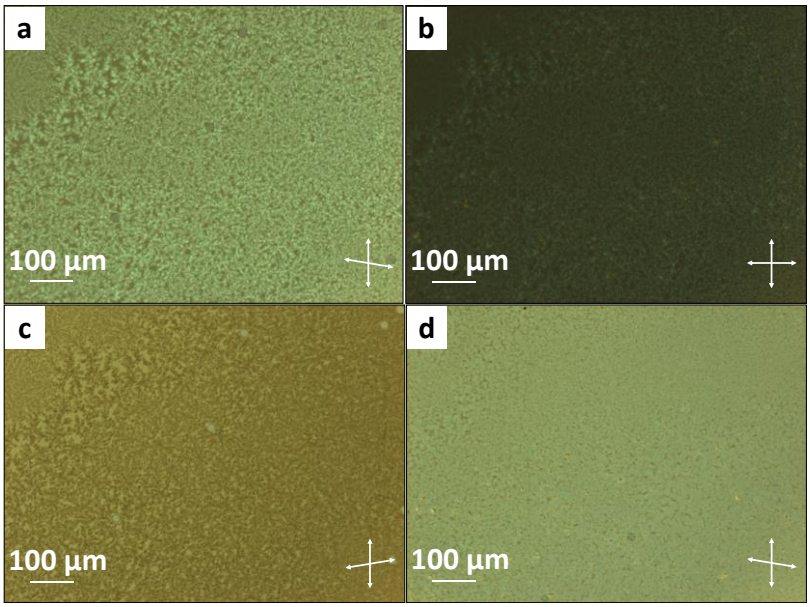

Fig. S22 POM textures of the compound **14F-4R** in coated cells with homeotropic anchoring, antiparallel rubbed with 18.3 µm thickness (a) and (c) showing opposite chirality domains observed under uncrossed polarizers (by 7° angle) and (b) crossed polarizer conditions, at 175.9 °C; (d) in crystalline phase at 93.9 °C.

5. Differential Scanning Calorimetry

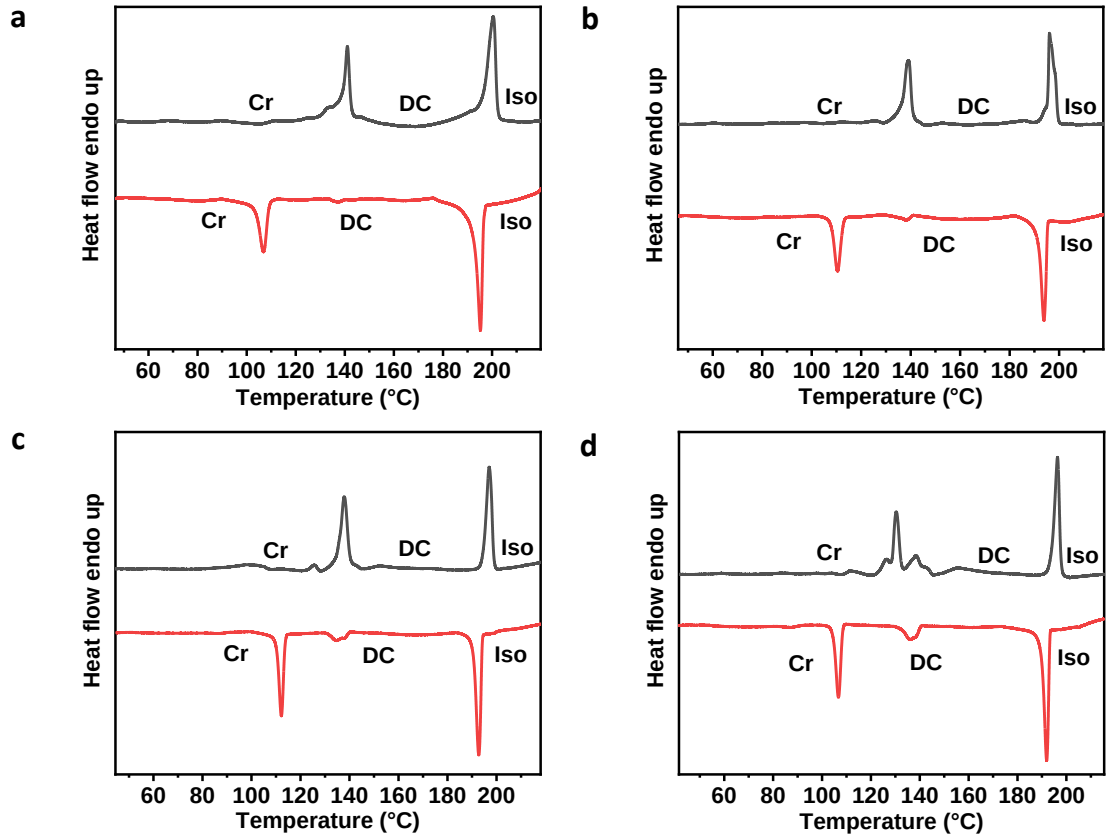

Fig. S23 DSC thermograms (after baseline correction) displaying transitions in both the heating (in black) and cooling (in red) cycles for (a) **12F-4R** (b) **14F-4R** (c) **16F-4R** and (d) **18F-4R**.

6. Atomic Force Microscopy

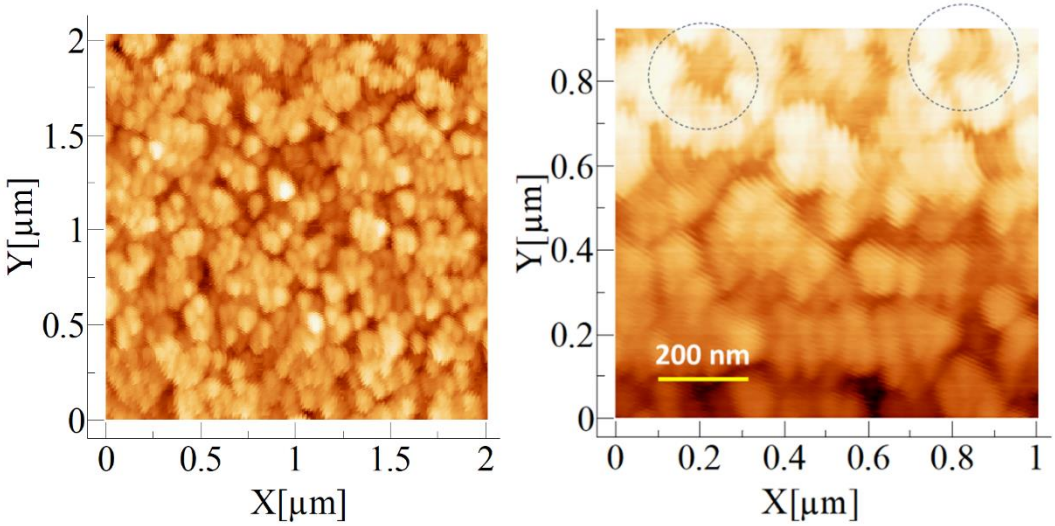

Fig. S24 AFM images obtained for **14F4R** sample quenched in the DC phase on an ITO-coated glass substrate.

7. Small-Angle and Wide-Angle X-ray Scattering

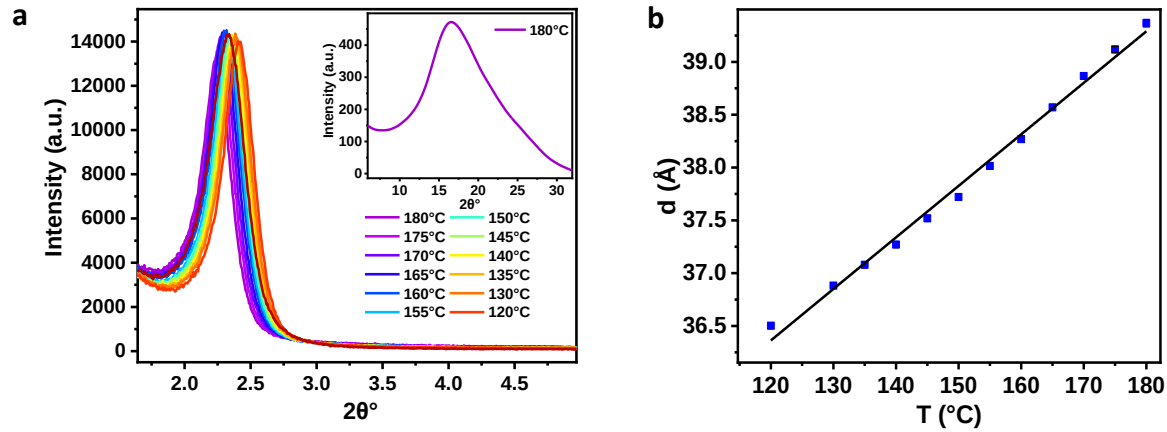

Fig. S25 (a) Temperature-dependent Intensity vs. 2θ plots for **14F-4R** in the small-angle and wide-angle (inset) regions. (b) Variation of *d*-spacing with respect to temperature for **14F-4R**.

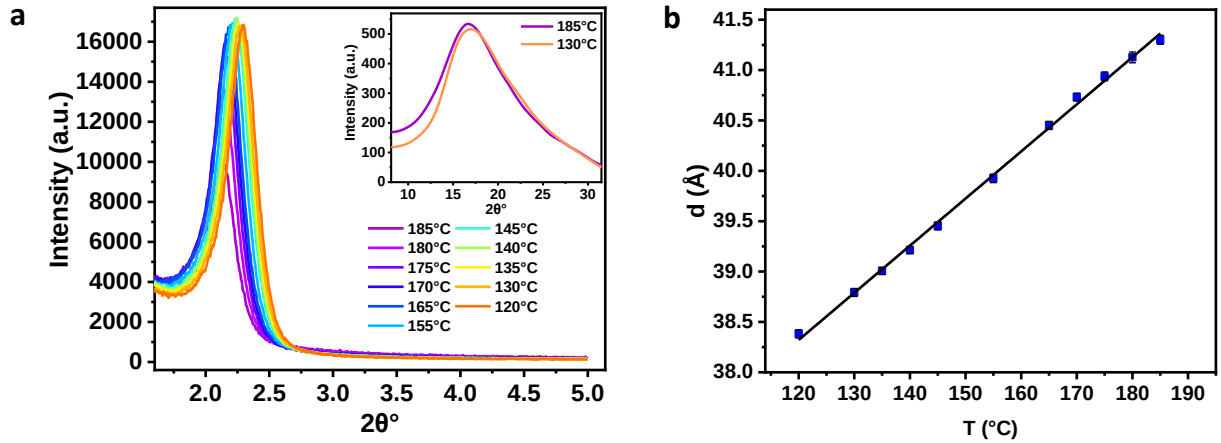

Fig. S26 (a) Temperature-dependent Intensity vs. 2θ plots for **16F-4R** in the small-angle and wide-angle (inset) regions. (b) Variation of *d*-spacing with respect to temperature for **16F-4R**.

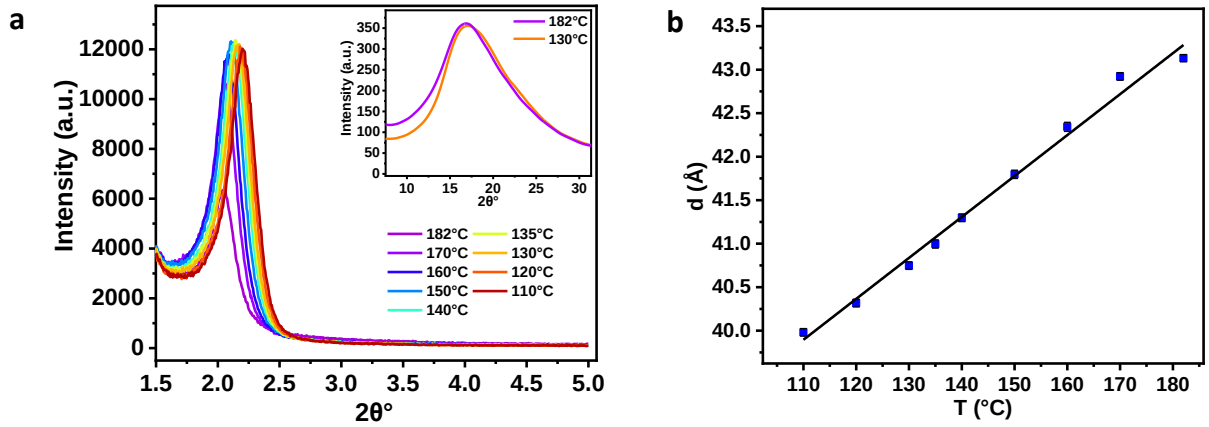

Fig. S27 (a) Temperature-dependent Intensity vs. 2θ plots for **18F-4R** in the small-angle and wide-angle (inset) regions. (b) Variation of *d*-spacing with respect to temperature for **18F-4R**.

Calculation for *d*-spacing and tilt-angle

The *d*-spacing can be calculated using Bragg's equation as follows:

$$\mathbf{2}\boldsymbol{d}\ \boldsymbol{sin}\boldsymbol{\theta} = \mathbf{n}\boldsymbol{\lambda}$$

Where θ is found from Intensity vs. 2θ plots, λ is the wavelength of the X-ray beam used and n = 1 for first-order diffraction. Further, the tilt-angle (θ) with respect to layer normal can be calculated using cosθ = *d*/L where L is the molecular length of the compound (obtained from DFT calculations).

Table S1 Temperature vs *d*-spacing for **nF-4R** series of compounds.

12F-4R		**14F-4R**	
Temperature (°C)	***d-value (Å)***	***Temperature (°C)***	***d-value (Å)***
185	37.2	180	39.4
180	37.0	175	39.1
170	36.7	170	38.9
160	36.3	165	38.6
150	35.8	160	38.3
140	35.4	155	38.0
135	35.2	150	37.7
130	35.0	145	37.5
120	34.6	140	37.3
110	34.4	135	37.1
		130	36.9
		120	36.5
16F-4R		**18F-4R**	
185	41.3	182	43.1
180	41.1	170	42.9
175	40.9	160	42.3
170	40.7	150	41.8
165	40.4	140	41.3
155	39.9	135	41.0
145	39.4	130	40.7
140	39.2	120	40.3
135	39.0	110	40.0
130	38.8	105	40.6
120	38.4		
110	39.3		

8. Dielectric measurements

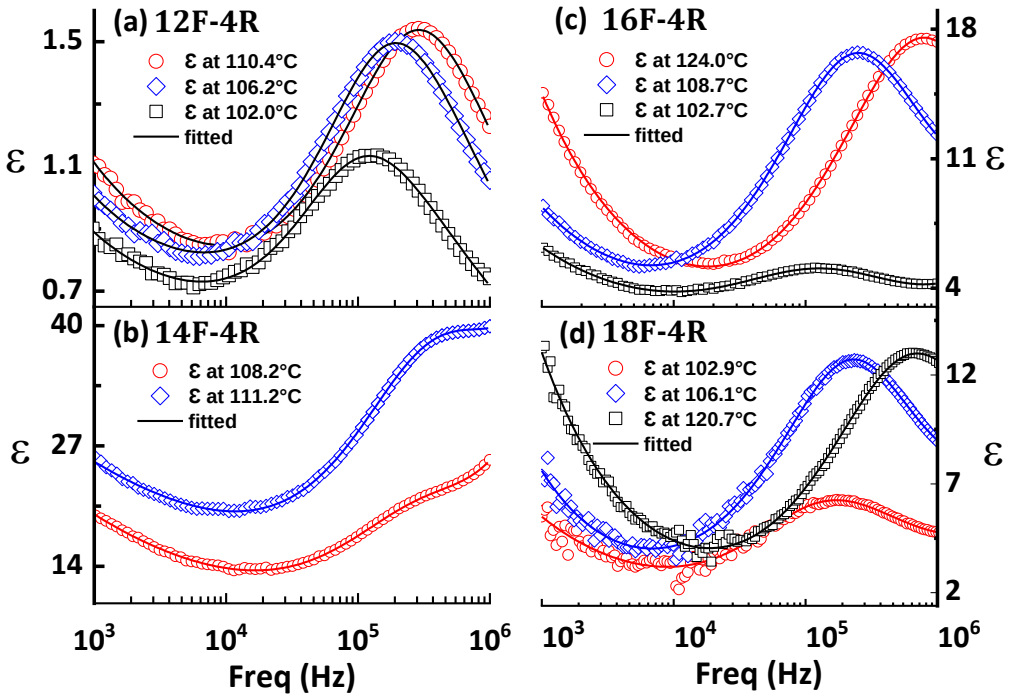

Fig. S28 Variation of imaginary part of the complex permittivity (epsilon), as a function of probing frequency (f) at representative temperatures for **nF-4R** compounds.

Table S2 Activation energy values for the relaxation process.

Compound	Activation energy E_A (kJ/mol)
12F-4R	117.3 ± 5.4
14F-4R	87.4 ± 2.4
16F-4R	93.1 ± 4.1
18F-4R	82.9 ± 1.4

9. Photophysical and Density Functional Theory studies

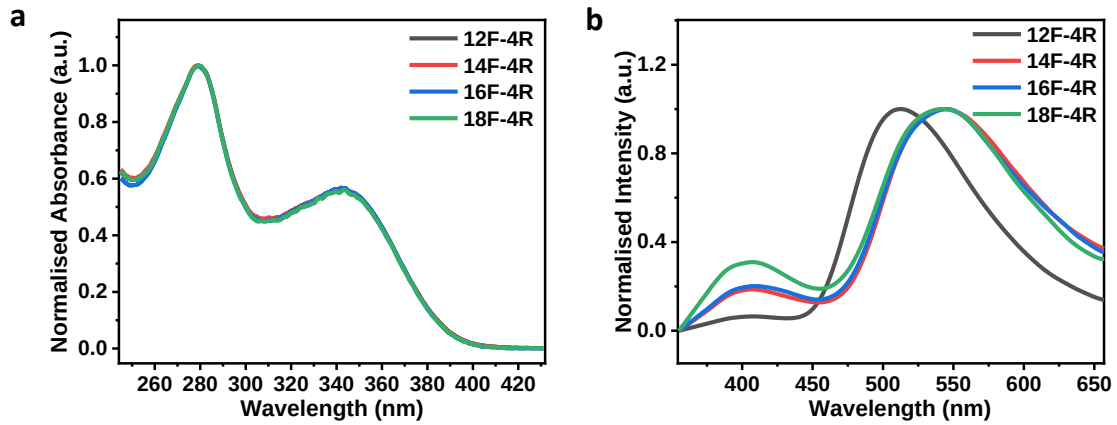

Fig. S29 Normalized UV spectra and Fluorescence Emission spectra for the **nF-4R** series of compounds.

To gain a thorough understanding of the optical properties and electronic transitions that occur during photoexcitation of LC materials, it is imperative to examine their absorption and emission characteristics. The UV-Vis spectra of the **nF-4R** series of compounds, recorded in a 5 x 10^{-3} M chloroform solution, revealed two distinct absorption peaks at 279 nm and 342 nm (Fig. S29a, ESI). These absorption bands can be attributed to different electronic transitions: the peak at 279 nm corresponds to a $\pi \rightarrow \pi^*$ transition, while the peak at 342 nm corresponds to an $n \rightarrow \pi^*$ transition. The lower absorption wavelength at 279 nm signifies a higher-energy electronic transition in these materials. Upon excitation at a wavelength of 342 nm, these materials exhibited fluorescence with an intriguing dual-emission behavior in their spectrum, providing valuable insights into their photophysical properties. The primary emission peak was prominently observed at 544 nm, accompanied by a secondary emission band around 407 nm (Fig. S29b, ESI). The occurrence of this dual emission behavior in the fluorescence spectra can be attributed to a phenomenon known as Excited-State Intramolecular Proton Transfer (ESIPT).[5] The **nF-4R** series of compounds incorporate a salicylaldimine linkage, which is known to exhibit keto-enol tautomeric equilibrium. Upon photoexcitation, ESIPT processes are driven, resulting in two distinct emission peaks. One emission peak originates from the keto tautomer, while the other emerges from the enol tautomer (usually less intense and at a lower wavelength than the keto form). The investigation of the photophysical properties of the **nF-4R** series contributes to the comprehension of the electronic and structural characteristics of bent-core LCs which aid in the development of novel liquid crystal materials with tailored optical properties, potentially finding applications in advanced displays, photonics, and sensors.

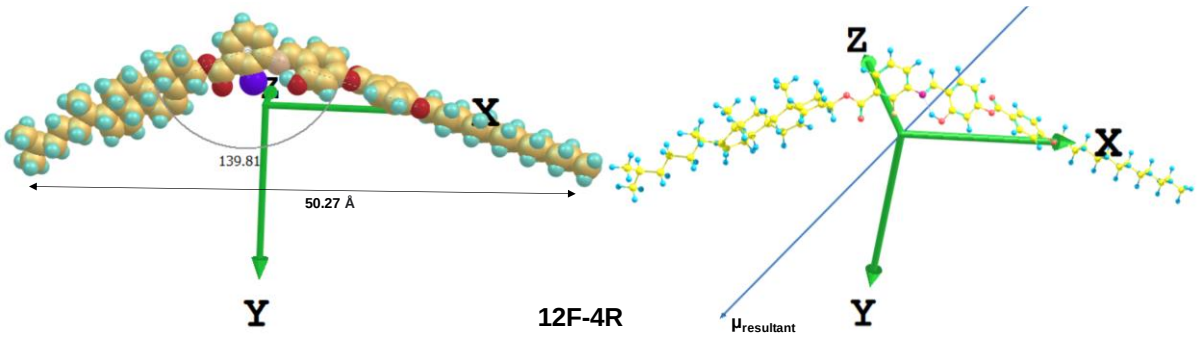

Fig. S30 DFT-optimized structures displaying bent angle, molecular length, and resultant dipole moment orientation for **12F4R**.

To gain insights into the molecular conformational geometry and electronic structure, Density Functional Theory (DFT) calculations were performed using Gaussian 16 and GaussView 5.0 package. Geometry optimizations, conducted with the B3LYP exchange-correlation functional and a 6-31g (d, p) basis set without geometry constraints, confirmed the bent molecular architecture of **nF-4R** molecules. The optimized DFT structure of **nF-4R** molecules revealed the bent molecular architecture featuring a bent angle of 139.5° and a molecular length of 50.27 Å. The optimised geometry of **12F-4R** is shown in Fig. S30, displaying the molecular conformation revealing non-coplanarity in shape and flexibility around the linking groups and also showing the direction of net dipole moment.[2] A resultant dipole moment value of ~3.7 D is observed in this series of compounds. The detailed information on the optimized geometries, bent angles, molecular lengths, and dipole moment values are provided in Fig. S31 and Table S3.

The electronic structure and energy characteristics of **nF-4R** compounds have been elucidated through the analysis of the Highest Occupied Molecular Orbital (HOMO), Lowest Unoccupied Molecular Orbital (LUMO), and the corresponding energy band gap. These parameters play a pivotal role in comprehending and optimizing a molecule's optical characteristics and assessing the stability of the molecular system. In the **nF-4R** series of compounds, it was observed that HOMO-LUMO orbitals are primarily localized near the core of the molecules (Fig. S32) and exhibit a HOMO-LUMO gap of 3.93 eV (Table S4). Such a large HOMO-LUMO gap signifies a higher energy threshold for electronic transitions, indicating enhanced kinetic stability in these compounds. The variations in charge density across the bent-shaped molecules have been mapped using electrostatic potential surfaces (Fig. S33), which illustrate distinct regions of both high and low electrostatic potential. High potential areas signify localized charge accumulation, while low potential regions indicate reduced electron density. This data provides valuable insights into the non-uniform charge distribution within the molecules, which in turn influences polarity, intermolecular interactions, and conformational stability. Understanding these comprehensive charge landscapes is essential for tailoring and fine-tuning the optical and dielectric properties of bent-core LCs to suit various applications.

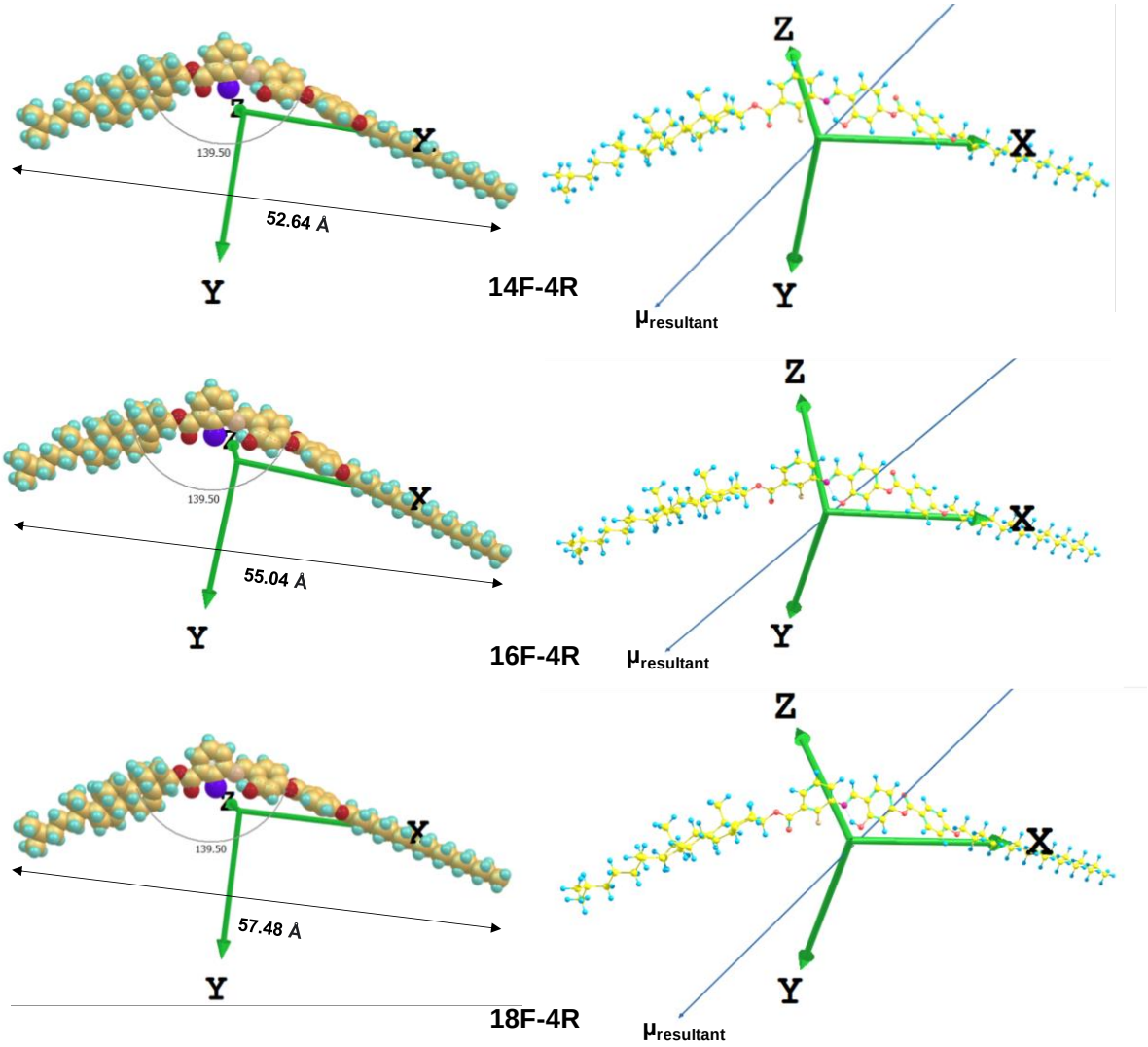

Fig. S31 DFT-optimized structures displaying bent angle, molecular length, and resultant dipole moment orientation.

Table S3 Dipole moments (in Debye) along X, Y, and Z directions, net dipole moment, Bend angle (°), and molecular length (Å).

Compound	μ_x	μ_y	μ_z	$\mu_{resultant} = (\mu_x^2 + \mu_y^2 + \mu_z^2)^{1/2}$	Bend-angle	Molecular Length, L
12F-4R	2.41	2.84	0.69	3.79	139.5	50.27
14F-4R	2.33	2.87	0.66	3.76	139.5	52.64
16F-4R	2.25	2.92	0.57	3.73	139.5	55.04
18F-4R	2.19	2.95	0.63	3.73	139.5	57.48

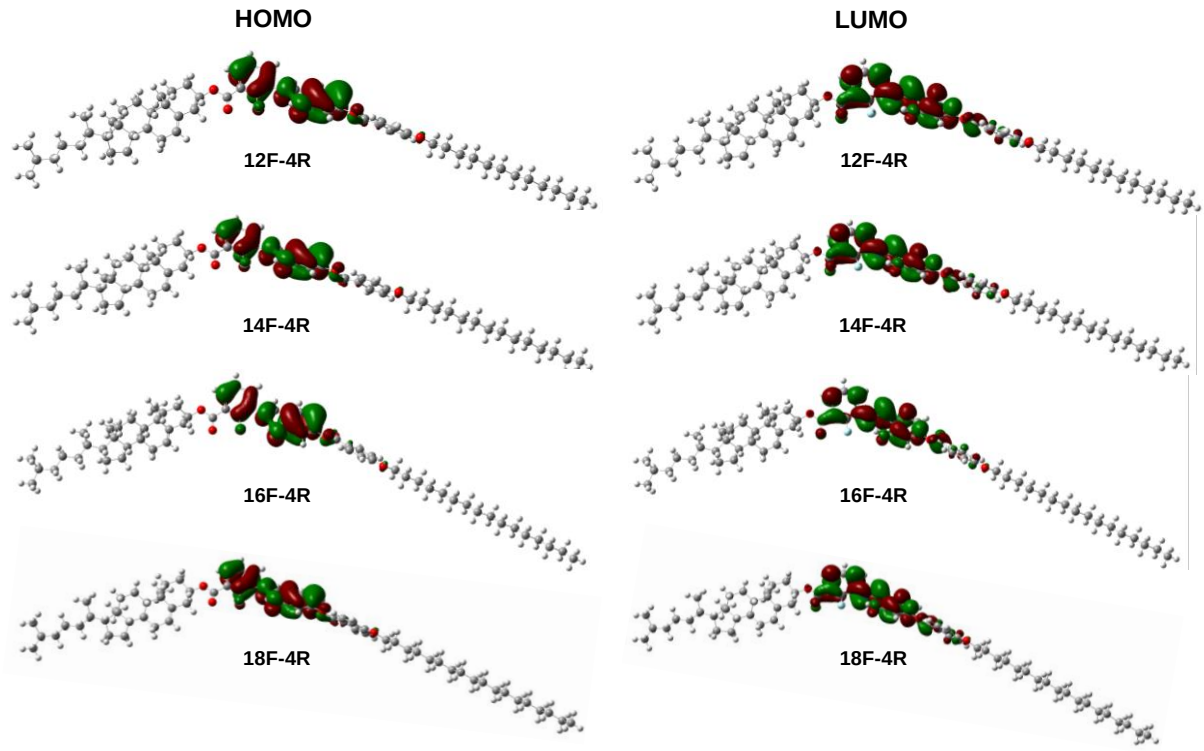

Fig. S32 HOMO and LUMO Molecular Orbitals of the **nF-4R** Series at Optimized Geometry.

Table S4 HOMO and LUMO Energy Levels (in eV).

Compound	HOMO (eV)	LUMO (eV)
12F-4R	-5.83	-1.90
14F-4R	-5.83	-1.90
16F-4R	-5.83	-1.90
18F-4R	-5.83	-1.90

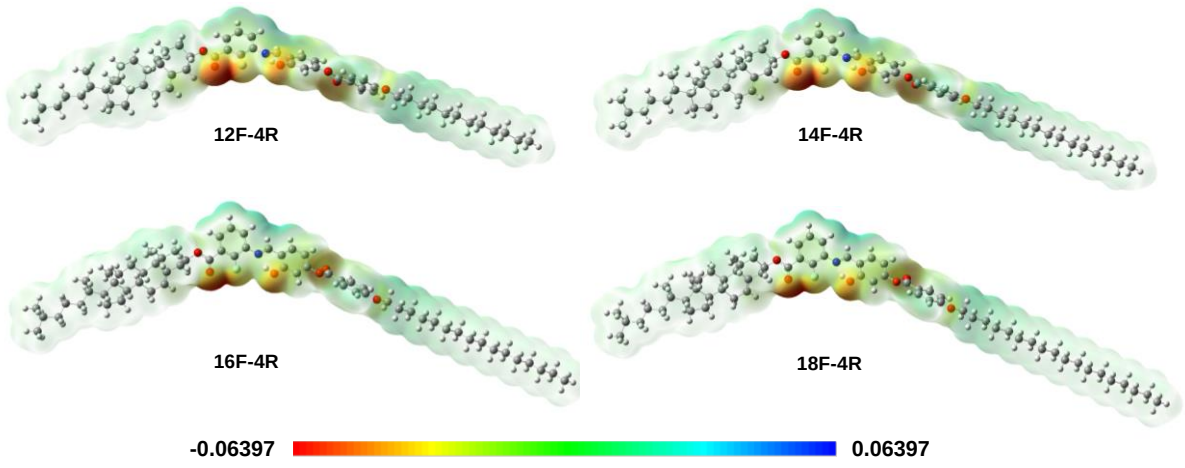

Fig. S33 Distribution of Molecular Electrostatic Potential.

10. References

1. S. Rani, V. Punjani, S. P. Gupta, M. B. Kanakala, C. Yelamaggad and S. K. Pal, *J. Mater. Chem.*, 2023, **11**, 1067-1075.
2. V. Punjani, G. Mohiuddin, S. Kaur, R. K. Khan, S. Ghosh and S. K. Pal, *Chem. Comm.*, 2018, **54**, 3452-3455.
3. I. Bala, N. Singh, R. A. K. Yadav, J. De, S. P. Gupta, D. P. Singh, D. K. Dubey, J.-H. Jou, R. Douali and S. K. Pal, *J. Mater. Chem.*, 2020, **8**, 12485-12494.
4. S. Kaur, A. Barthakur, G. Mohiuddin, S. P. Gupta, S. Dhara and S. K. Pal, *Chem. Sci.*, 2022, **13**, 2249-2257.
5. A. K. Satapathy, S. K. Behera, R. Kumar, K. L. Sandhya, C. V. Yelamaggad and B. Sahoo, *Journal of Photochemistry and Photobiology A: Chemistry*, 2018, **358**, 186-191.